Nanoscale

MINIREVIEW

View Article Online
View Journal | View Issue

Cite this: *Nanoscale*, 2025, **17**, 15648

Fullerene-driven photocarrier processes in perovskite solar cells: recent advances

Muhammad Waqas,[a] Dhruba B. Khadka,[b]* Abdul Haseeb Hassan Khan[a] and Ying-Chiao Wang[a]*

This review highlights recent advances in elucidating the photocarrier dynamics of fullerenes in perovskite solar cells (PSCs). Fullerenes and their derivatives serve a critical role in facilitating charge transport, suppressing recombination losses, and enhancing device stability, with particular focus on their influence at the photocarrier level. The interfacial interactions between fullerenes and perovskite photoabsorbers are pivotal for efficient carrier extraction, where the distinctive electronic properties of fullerenes promote effective charge separation and transport. Recent spectroscopic developments have significantly deepened our understanding of charge generation, transport, and recombination mechanisms within PSC architectures. Moreover, functionalized fullerene derivatives have been strategically engineered to optimize energy level alignment, mitigate interfacial losses, and improve overall photovoltaic performance. These advancements collectively contribute to the development of more efficient and stable PSCs, driving progress toward next-generation solar energy technologies with enhanced photocarrier dynamic performance.

Received 9th May 2025,
Accepted 13th June 2025

DOI: 10.1039/d5nr01894c

rsc.li/nanoscale

1. Introduction

Organic–inorganic halide perovskite solar cells (PSCs) have emerged as a leading photovoltaic (PV) technology, demonstrating record-high power conversion efficiencies (PCEs),[1–3] along with the advantages of scalable processing[4] and low-cost fabrication routes.[5,6] Despite these advancements, the commercialization of PSCs remains hindered by key challenges, including inefficient charge transport,[7] significant recombination losses,[8] and long-term operational instability.[9] Among the factors governing device performance, photocarrier dynamics-encompassing charge generation, separation, transport, and recombination-play a central role in determining overall efficiency. In this context, fullerenes have attracted considerable attention due to their high electron affinity[10,11] and excellent charge mobility, positioning them as essential electron-transport materials (ETMs) for improving photocarrier behavior and device performance.

Fullerenes possess a unique cage-like structure[12] composed predominantly of hexagons,[13] pentagons,[14] and occasionally heptagons, with inherent molecular curvature[15] that critically influences their optical, electronic, and chemical properties.[16–18] This structural versatility allows for precise chemical functionalization, making fullerenes highly adaptable materials for optimizing PV performance in PSCs. Notably, fullerenes have demonstrated the ability to effectively passivate defect states (DSs) at both perovskite interfaces[19] and grain boundaries,[20] where the formation of fullerene-halide radicals plays a key role in suppressing deep-level trap states,[21] which are major contributors to charge-carrier trapping and nonradiative recombination losses. Beyond defect passivation, fullerenes significantly enhance electron transfer kinetics, thereby reducing hysteresis and improving the dynamics of photogenerated charge carriers.[22,23] Their relatively large molecular size enables them to physically occupy grain boundaries, hindering halide ion diffusion and thus mitigating ion migration pathways,[21,24] a critical factor in improving operational device stability.[25,26] Furthermore, chemical modification of fullerenes with polar functional groups such as hydroxyl,[27] carboxyl,[28] or amino moieties[29] has been shown to enhance solubility, environmental stability, and interfacial compatibility with perovskite layers-collectively contributing to finely tuned charge dynamics and improved device performance.

The incorporation of fullerene derivatives has played a pivotal role in advancing the efficiency of PSCs, with fullerene-based ETMs enabling PCEs of up to 22%.[30] Nevertheless, recent advancements employing non-fullerene ETMs have surpassed the 25% efficiency threshold,[31] underscoring the rapid

[a]*Department of Materials and Optoelectronic Science, National Sun Yat-sen University, Kaohsiung, 804 Taiwan, Republic of China. E-mail: ycwang@mail.nsysu.edu.tw*
[b]*Photovoltaic Materials Group, Center for GREEN Research on Energy and Environmental Materials, National Institute for Materials Science (NIMS), 1-1 Namiki, Tsukuba, Ibaraki 305-0044, Japan. E-mail: KHADKA.B.Dhruba@nims.go.jp*

evolution and diversification of ETM materials in next-generation PSC architectures.[31]

Functionalized fullerenes exhibit multifunctional properties that extend beyond their conventional role as ETMs. In particular, they contribute to defect passivation at the perovskite/ETM interface and within grain boundaries, thereby suppressing non-radiative recombination pathways and promoting improved perovskite crystallinity during film formation.[32,33] The resulting enhancement in film uniformity not only facilitates more efficient light harvesting but also contributes to prolonged device operational lifetimes.[34] Moreover, fullerenes provide an effective barrier against moisture and oxygen ingress, addressing key environmental degradation pathways and significantly improving the long-term stability of PSCs under ambient conditions.[30,35]

Despite these advantages, challenges such as molecular aggregation[36] and residual ion diffusion[32] persist in fullerene-based electron transport layers. To address these limitations, cross-linkable fullerene derivatives have been developed, forming robust molecular networks that suppress aggregation and act as effective barriers against ion migration-thereby enhancing both the efficiency and operational stability of PSCs.[11] This review summarizes recent progress in the application of fullerenes in PSCs, with a particular focus on the interplay between fullerene molecular structures and device performance. By examining the latest strategies in fullerene design and functionalization, we provide insights into the optimization of charge-carrier dynamics within perovskite architectures. Continued innovation in fullerene chemistry and its integration into PSCs holds substantial promise for advancing high-efficiency, stable, and commercially viable next-generation photovoltaic technologies.

2. Carrier dynamics regulation

In high-performance PSCs, charge transport layers (CTLs) play a pivotal role in device operation by: (1) facilitating efficient charge carrier extraction, (2) promoting the formation of high-quality perovskite films with reduced defect densities,[36–38] and (3) enabling flexible device architectures. For instance, interface-engineered CTLs have enabled PSCs to achieve PCEs exceeding 23% on flexible polyethylene terephthalate (PET) substrates.[39]

To achieve such performance, optimizing the interfaces between the ETM and perovskite, as well as between the perovskite and hole transport material (HTM), is essential for enhancing charge generation, promoting efficient extraction, and suppressing non-radiative recombination losses. These interface improvements are commonly realized through perovskite composition engineering, surface/interface passivation strategies-such as fullerene-based interlayers-and CTL bandgap tuning to ensure favorable energy-level alignment (ELA).[40,41] Furthermore, the internal electric field, generated by the ΔE between the highest occupied molecular orbital (HOMO) level of the HTM and the lowest unoccupied molecular orbital (LUMO) level of the ETM,[42] plays a crucial role in facilitating exciton dissociation at the respective interfaces. In well-optimized devices, this built-in potential enables charge separation efficiencies exceeding 90%, while also promoting the diffusion and separation of photo-generated carriers

Muhammad Waqas

Muhammad Waqas is currently pursuing his Ph.D. in the Department of Materials and Optoelectronic Science at National Sun Yat-sen University under the supervision of Professor Ying-Chiao Wang. His research focuses on the development of nanomaterials and their application in photovoltaic devices.

Ying-Chiao Wang

Prof. Ying-Chiao Wang is currently an Assistant Professor in the Department of Materials and Optoelectronic Science at National Sun Yat-sen University, Taiwan, R.O.C. He received his Ph.D. in Materials Science from National Taiwan University in 2015. From 2016 to 2018, he held a distinguished young researcher position at the Ningbo Institute of Material Technology & Engineering, Chinese Academy of Sciences. In 2018, he worked as a postdoctoral researcher at Nagoya University and was later selected as an ICYS Research Fellow at the National Institute for Materials Science (NIMS), Japan. From 2021 to 2022, he continued postdoctoral research at International Center for Materials Nanoarchitectonics (MANA), NIMS. In 2022, he joined iLab, Foxconn Technology Group, as a materials engineer. His research focuses on solution-processed nanomaterials for photovoltaic applications.

throughout the active layer. Thus, careful bandgap alignment at the ETM/perovskite/HTM interfaces is imperative to minimize energetic barriers and ensure efficient and balanced charge transport across the device.[43,44]

2.1 Device structure

PSCs leverage perovskite materials' unique properties to convert light into electrical energy.[45] A typical device comprises an electrode supporting an n-type ETM, (compact or mesoporous), a perovskite light-harvesting layer, and a p-type HTM. Upon light absorption, the perovskite excites electrons to its LUMO, forming excitons that dissociate at the ETM/perovskite and perovskite/HTM interfaces (Fig. 1a).[46] Free electrons transfer to the ETM and holes to the HTM (Fig. 1b), with selective transport reducing recombination. Electrons collect at the anode, flow through an external circuit, and recombine with holes at the cathode. The ETM selectively transports electrons while blocking holes, and conversely, the HTM transports holes while blocking electrons. This selective transportation ensures efficient charge separation and minimizes recombination losses. The free electrons are subsequently gathered at the anode, where they traverse an external circuit, thereby producing an electric current. Finally, at the cathode, the electrons recombine with holes, completing the circuit. The effectiveness of this process is significantly enhanced by the perovskite material long diffusion lengths (L) and high carrier mobilities ($\mu_{n,p}$), enabling efficient charge separation and transport. PSCs can be manufactured using two distinct methods. These methods vary based on the order of deposition for the materials involved, either the ETM is applied first, or the HTL is applied first, (Fig. 1(c and d)). The choice of method influences the overall performance and characteristics of the device. In the standard architecture for conventional NIP-type configurations, an n-type ETM is placed beneath an insulating light-harvesting layer, with a p-type HTL situated above it (Fig. 1d).[46] This arrangement forms an (ETM/perovskite/HTL) stack. Conversely, the inverted PIN-type architecture features a p-type HTL at the base, an insulating light-harvesting layer in the middle, and an n-type ETM on top, resulting in an (HTL/perovskite/ETM) configuration (Fig. 1e). These two configurations will be conferred in the following section.

2.1.1 NIP configurations. The NIP diode, characterized by its N-type (N), intrinsic (I), and P-type (P) layers, is a highly adaptable semiconductor device extensively employed in electronic and optoelectronic technologies.[52] Unlike conventional diodes, which contain only N–P junctions, the NIP diode includes a substantial intrinsic layer between the N-type and P-type regions.[53] This intrinsic layer is crucial for its unique operational characteristics, such as low capacitance and high-speed switching capabilities, making NIP diodes indispensable in high-frequency applications and photodetection.

Understanding the operation of an n–i–p diode requires a foundational knowledge of the photo-induced charge carriers interface.[54] The creation of the charge carrier junction in an NIP diode requires the doping of semiconductor material to establish regions with excess positive (P-type) and negative (N-type) charge carriers. The intrinsic (I) layer, undoped and positioned between these two regions, plays a pivotal role in the diode functionality. When a potential difference is applied across the NIP diode, the electric field spans the intrinsic region, resulting in the formation of an extensive depletion zone. This depletion region is essential for the diode high-speed switching and low capacitance, as it allows the diode to quickly respond to changes in the applied voltage without the significant charge storage issues found in conventional diodes. In photovoltaic applications, the width of the depletion

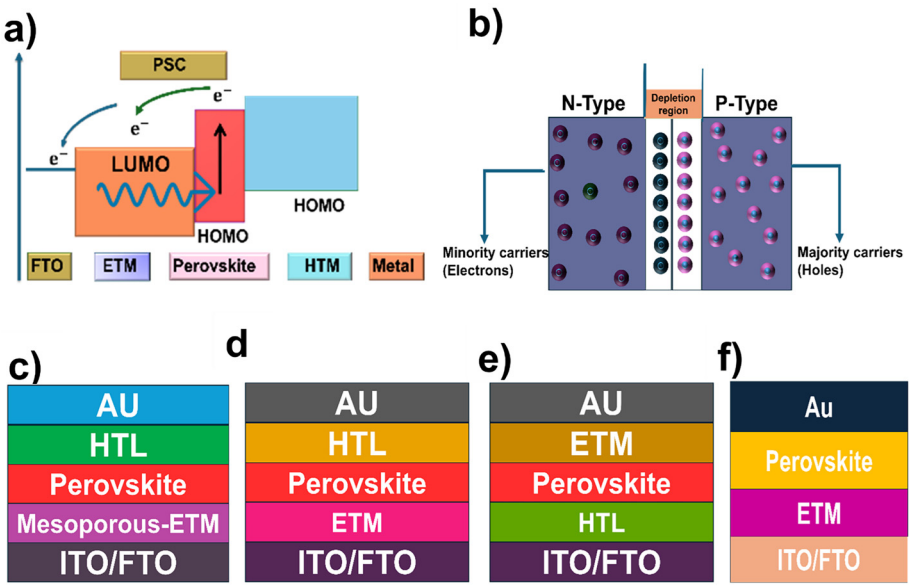

Fig. 1 (a) Working principle of PSC,[47] (b) PN-junction,[48] (c) mesoporous configuration,[49] (d) NIP configuration, (e) PIN configuration,[50] and (f) HTL-free PSC.[51]

region plays a key role in the PCE.[55] A narrow depletion region, often found in conventional diodes, poses several challenges.[56] Firstly, it leads to higher capacitance, which hampers the diode ability to operate effectively at high frequencies. Secondly, and more critically for photovoltaics, narrow depletion regions are less efficient in separating and collecting excitons generated under incident illumination.[57] This inefficiency in charge carrier separation results in lower responsivity and conversion efficiency, ultimately limiting the effectiveness of PSCs relying on these diodes.[58] In contrast, the NIP diode's wide depletion region offers significant advantages for photovoltaic applications.[59] An extensive intrinsic region may lead to a slower response speed due to the increased distance for electrons and holes to travel and recombine.[60]

2.1.2 PIN configuration. The PIN structure, a variant of the NIP configuration, comprises layers arranged sequentially as a p-type layer, an insulating or intrinsic layer, and an n-type layer.[61] The intrinsic (I) layer plays a critical role in enabling efficient photon absorption and generating charge carriers.[62] The absorber materials that are composed of perovskite can effectively absorb a broad spectrum of photons that generate electron–hole pairs (excitons), which contribute to a PCE of 24%, as reported in Table 1. The layer quality impacts charge separation and transport, with advancements in perovskite synthesis enhancing crystallinity, reducing defect density, and enhancing stability, ultimately boosting the PCE and thermal stability of NIP PSCs.[63]

2.1.3 HTL free PSCs. PSCs primarily rely on multiple CTLs, including ETMs and HTLs. The frequently utilized inorganic HTLs are 2,2′,7,7′-tetrakis(*N*,*N*-*p*-dimethoxyphenylamino)-9,9′-spirobifluorene (Spiro-OMeTAD), polytriarylamine (PTAA), and nickel oxide (NiO_x), *etc*. These materials significantly contribute to the effective collection and transfer of charge carriers. However, the inclusion of HTLs introduces several challenges, including material instability which is a significant concern, as HTLs, particularly Spiro-OMeTAD, are susceptible to chemical and thermal degradation, which impacts device stability,[70,71] also NiO_x, which is characterized by a high concentration of Ni^{3+}, can accept electrons from tin perovskites. This interaction facilitates the oxidation of Sn^{2+} to Sn^{4+}, which ultimately leads to diminished stability in Ni-based tin PSCs.[69,72] Additionally, the hygroscopic nature of numerous HTL materials leads to moisture absorption from the environment, hastening the degradation of the light-harvesting layer.[73,74] The low hole mobility of commonly used HTL materials further hampers efficient charge transport, reducing overall device performance.[75] Moreover, perovskites possess long carrier diffusion lengths, often exceeding several hundred nanometers.[76] These characteristics enable efficient charge separation and extraction within the light-harvesting layer, theoretically reducing the need for separate ETMs and HTLs.[77]

Due to the bipolar nature and extended carrier diffusion length of perovskites, the presence of an ETM and an HTL is not essential for the mechanisms of charge separation and extraction. In an optimal configuration, as described by Kim and Liu *et al*. the light-harvesting layer alone would be sufficient to gather and transport charge carriers to the respective electrodes with minimal losses.[78,79] This concept has led to the exploration of HTL-free PSC configurations (Fig. 1f), aiming to simplify device architecture and reduce manufacturing costs.

In recent years, significant efforts have been directed toward the development of PSCs without the HTL layer.[80] Etgar *et al.* were the first to propose the successful fabrication of HTL-free PSCs, demonstrating that the $CH_3NH_3PbI_3$ ($MAPbI_3$) crystal could function both as a hole conductor and a light absorber, (Fig. 2a). Zhang *et al.* improved the ELA by creating a layered perovskite structure composed of $MAPbI_3$/$MAPbI_xBr_{3-x}$. The valence band maximum (VBM) of $MAPbI_xBr_{3-x}$ was 0.23 eV higher than that of $MAPbI_3$, facilitating hole extraction by reducing the energy barrier (Fig. 2b). At the same time, the conduction band (CB) of $MAPbIxBr_{3-x}$ was found to be 0.25 eV higher than that of $MAPbI_3$ (Fig. 2c), which hindered the electron transfer from the light-harvesting layers to the carbon electrode.

2.2 Charge transport layer engineering

In PSC devices, the behavior of photoinduced excitons is predominantly governed by the attributes of the active layer.[85] Moreover, the performance of a PSC is contingent upon its proficiency in capturing incident photons, as well as the effectiveness of charge transport and collection at the corresponding electrodes.[86,87] Various elements that influence light propagation and charge transport within the device, such as energetic barriers at interfaces, the existence of defect states in the light-harvesting layer or adjacent functional layers, and parasitic absorption, will impose limitations on the overall performance of the device. Recently, the PCE of PSCs has witnessed advancements driven by the strategic implementation of interface engineering. This approach involves the incorporation of distinct interfacial materials between the ETM/HTL and perovskite active layer.[41,73] The introduction of interfacial materials serves two primary functions: ELA and chemical modification.

Table 1 Device data of NIP,[64,65] PIN,[66,67] mesoporous[68] and HTL-free configurations[69]

Device configuration	Perovskite	ETM	HTM	PCE (%)	Stability
NIP	$MAPbI_3$	TiO_2	Spiro-OMeTAD	21–26.42	80%
PIN	$FA_{0.90}MA_{0.10}PbI_3$	SnO_2	NiO	23.1–26.14	85%
Mesoporous	$(FAPbI_3)_{0.97}(MAPbBr_3)_{0.03}$	TiO_2	Spiro-OMeTAD	25.5	96.6%
HTL-free	Pb perovskite	TiO_2		10–11	90%

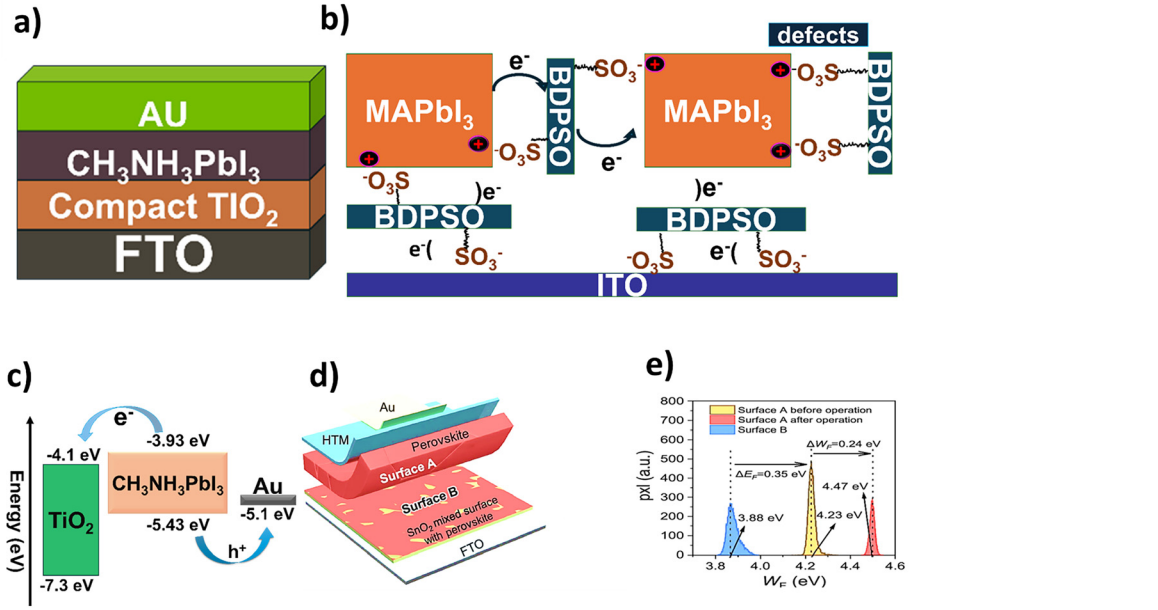

Fig. 2 (a) Device representation of HTL-free PSC.[81] (b) A schematic representation depicting the influence of BDPSO dopants in HTL-free PSC.[82] (c) Energy states diagram of HTL-free PSC, (d) a schematic illustration of the separation at the buried interface of the PSC. The inset displays the use of a KPFM or AFM probe for measuring the work functions (WFs) of surface A and surface B.[83] (e) The WF distribution of surface A before and after operation, compared with surface B, is presented the SnO_2 surface was modified with $-C_3{\equiv}N$.[84]

2.2.1 Optimization of energy levels. To enhance the photo-induced charge carrier's dynamics in PSCs, carrier transport layers, such as the ETM and HTL, are typically incorporated on either side of the perovskite active layer. However, an energy level mismatch between the charge carrier transport layers and the perovskite can lead to energy losses at the interfaces. Thus, precise control of the interface ELA is essential for optimizing the photovoltaic parameters. Probing the ELA between the perovskite layer and the neighboring transport layers necessitates a detailed assessment of the energy level offset and the relative positions of their Fermi energy levels (FEL). The electronic states offset at the interface play a critical role in affecting interfacial recombination and dynamics of carrier infusion. The positioning of the FEL determines the alignment and extent of energy band bending at the interface, which in turn influences the efficiency of charge carrier extraction. Moreover, the FEL of the perovskite and adjacent layers significantly affects the quasi-FEL splitting in PSCs, thereby influencing the maximum achievable photovoltage. Therefore, to attain the best possible performance from the device, it is essential to carefully evaluate these factors.

In PSCs, defect-assisted recombination primarily arises from Shockley–Read–Hall (SRH) recombination and interfacial recombination mechanisms, (Fig. 3). These processes are critical in determining the overall efficiency of charge carriers.[88,89] SRH recombination in light-harvesting layers is primarily instigated by the presence of uncoordinated ionic defects, which give rise to deep-level defect states. These DSs are energetically positioned within the bandgap and can capture free charge carriers, effectively impeding the charge dynamics, and thereby increasing defect-assisted recombination (Fig. 3b). This process results in significant energy losses, as the trapped carriers recombine without contributing to photovoltaic output.

Non-emissive recombination in PSC primarily occurs due to mismatched energy levels or DSs leading to thermal potential loss and significantly reducing the open-circuit voltage (V_{oc}) and fill factor (FF).[91] This misalignment causes thermal potential loss and primarily reduces the V_{oc} and FF of the devices. Therefore, the suitable energy levels of the ETM as well as HOMO/LUMO, are critical parameters for device performance.[92] A high-quality ETM with appropriate energy levels facilitates efficient electron transport and hole blocking, enhancing overall efficiency.

The collection of charge carriers by HTLs or ETMs occurs *via* the built-in electric field (E_{bi}). The energy offsets (ΔE) between the LUMO level of ETM and the HUMO level of HTL are critical for minimizing non-emissive recombination. Lower values of ΔE_1 of the valence band and ΔE_2 of the CB decrease recombination rates, while higher values increase them. Optimal band offsets, ideally below 0.2 eV, enhance charge transport and reduce interface recombination. Therefore, the selection of the conduction or valence band of the HTL/ETM, or the LUMO/HOMO for molecular CTLs, is critical to ensure selective charge extraction. This is achieved by establishing an energetic barrier that effectively facilitates the specific extraction of electrons or holes, thereby boosting the efficiency and performance of the device.

2.2.2 Tuning charge dynamics at the interface through chemical engineering. Interface layers (ILs) extend their influ-

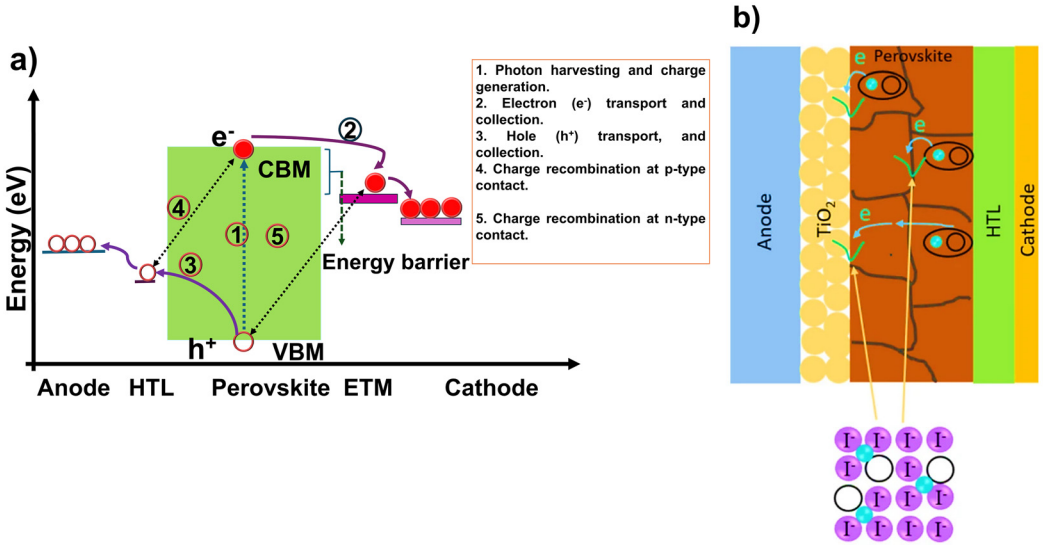

Fig. 3 (a) The mechanism of radiative recombination of photo-induced charge carriers,[86] and (b) defect recombination mechanism at ETM/perovskite interface.[90]

ence beyond optimizing ELA. They possess the valuable capability to passivate defects and traps residing at the active layer surface or interface.[57] Passivation involves applying a protective layer, typically a material that chemically interacts with the base substrate, to form a micro-coating that provides protection. The transition from an active to a passive state is achieved through the creation of this passivation layer. In PSCs, passivation typically arises through two mechanisms: chemical passivation and physical passivation.[93,94] Chemical passivation focuses on minimizing DSs to improve charge transfer across interfaces, while physical passivation involves shielding specific functional coatings from environmental exposure to prevent cell degradation. These passivation techniques are essential for optimizing PSCs, resulting in improved PCE and overall performance.

The interface between the CTL and the perovskite may exhibit weak adhesion because of inhomogeneities in composition and the presence of strain within the light-harvesting layer. Such inhomogeneities could potentially result in a diminished homojunction of the perovskite next to the CTLs. The potential for a WF discrepancy at the perovskite homojunction as, characterized by weak adhesion, suggests that the interface may adversely affect stability. Thus, it is imperative to regulate the WF to improve overall stability, (Fig. 2d). Consequently, there is a need to explore strategies for assessing the WF of the weak homojunction within the light-harvesting layer that is situated near the CTL. The n–i–p configuration featuring a SnO_2 CTL detachment of the perovskite layer from the SnO_2-coated fluorine-doped tin oxide (FTO) substrate may serve as an effective approach to assess the WF of the weakly adhering homojunction. The light-harvesting layer was partially removed from the SnO_2-coated FTO substrate; however, a residual thin layer of perovskite remained attached to the SnO_2 surface. The bottom surface of the perovskite film and the top surface of the SnO_2 film were identified as "surface A" and "surface B", respectively. The WF values for surface A and surface B were measured at 4.23 eV and 3.88 eV, respectively, (Fig. 2e), as determined by a kelvin probe force microscope (KPFM). This variation in WF indicates the formation of a homojunction.

3 Recent progress in ETMs

In PSCs, the ETM is situated between the metal electrode and the light-harvesting layer.[95] This layer plays a crucial role in modifying the interface by generating an interfacial dipole, which subsequently alters the vacuum level. Such modifications facilitate electron extraction by reducing the energy barrier at the interface. By establishing an efficient connection between the metal electrode and the photovoltaic active layer, the ETM effectively minimizes energy losses and recombination during charge extraction, thus enhancing the PCE of PSC.[32] A promising ETM is characterized by well-aligned energy levels with the light-harvesting layer. Specifically, having its LUMO/HOMO positioned elevated than those of the perovskite layer. Furthermore, the ETM should demonstrate high transmittance in the UV-Vis spectrum to ensure that photons can easily penetrate the perovskite absorbed by it. The evaluation of transmittance, absorption spectra, mobility, and conductivity are used to assess the optical and electronic properties.

3.1 Metal oxides (MOs) based ETMs

In recent years, the development of metal oxides (MOs) has been preferred as ETMs due to their facile fabrication process,[96] high intrinsic stability, tunable optical and electronic properties,[97] low-temperature or no post-treatment

requirements,[70] low cost, and additional passivation function. These benefits enhance their application in high-performance inverted PSCs.

3.1.1 Titanium oxide (TiO_2). TiO_2 has garnered significant attention as an ETM due to its advantageous positions (HOMO/LUMO) that facilitate the extraction and injection of charge carriers. Its high electron mobility, appropriate energy levels, and robust chemical stability further contribute to its suitability as an ETM.[98–100] Khan *et al.* achieved 22.10% PCE using TiO_2 as ETM with $CsSnI_2Br$ based PSC using numerical calculations.[101] However, TiO_2 faces several challenges, particularly its high processing temperatures and photocatalytic activity, which can degrade device stability.[102,103] Recent studies have attempted to overcome these limitations through doping and nanoengineering. Doping TiO_2 with elements such as nitrogen and fluorine has enhanced its electrical conductivity and light absorption properties, while nanoengineering approaches like creating nanorods and nanotubes have improved electron transport and reduced recombination losses.[104] Despite these advancements, there are still some issues with TiO_2 as an ETM material, such as UV degradation. Upon exposure to light, TiO_2 undergoes bandgap excitation, leading to the generation of electron–hole pairs.[105,106] The photoexcited electrons can migrate to the surface of the TiO_2, where they interact with the adsorbed oxygen molecules.[107] This phenomenon can induce the desorption of oxygen species from the surface, thereby destabilizing the charge transfer complex. The consequent depletion of surface-adsorbed oxygen species, crucial for passivating surface defects on TiO_2, results in the proliferation of recombination centers.[102] Consequently, this leads to a degradation of photocurrent and overall device performance. Additionally, the high processing temperatures required for TiO_2, exceeding 450 °C, pose a significant challenge, particularly for applications that involve flexible PSC devices.[79]

3.1.2 Zinc oxide (ZnO). The requisite high processing temperatures for TiO_2 constrain its utility as an ETM for PSCs. Consequently, ZnO's suitability for low-temperature processing renders it an auspicious candidate for the ETM in flexible PSCs, additionally providing a cost-effective alternative to the high-temperature sintering demanded by TiO_2.[108] ZnO has demonstrated superiority over TiO_2 as an ETM, attributable to its elevated electron mobility (Table 2) that enables rapid electron transport. Among the various deposition techniques for ZnO ETLs in planar PSCs, solution-based methods such as the sol–gel process have been extensively investigated. In 2014, Qiu *et al.* reported the fabrication of planar PSCs employing sol–gel-derived ZnO ETLs, achieving a PCE of 8.37%.[109–111]

Recently, there has been a significant surge in interest in developing low-temperature processable PSCs, driven by the escalating demand for this cutting-edge technology in the photovoltaic industry. ZnO is one of the most promising candidates and is extensively studied due to its superior optoelectronic properties compared to TiO_2, providing numerous advantages, especially in the realm of charge dynamics. ZnO can be processed at much lower temperatures compared to TiO_2, making it compatible with flexible and organic substrates. ZnO demonstrates superior electron mobility, enhancing charge transport efficiency and minimizing recombination losses. This higher mobility is partly due to ZnO intrinsic properties and its ability to form various nanostructures, such as nanorods, nanowires, and nanoparticles, which enhance the surface area and improve electron extraction. Recent advancements in ZnO ETMs include doping with elements like aluminum and gallium to further increase conductivity and reduce defects and developing composite materials that combine ZnO with other oxides or organic molecules to improve performance and stability. Surface passivation techniques have also been employed to mitigate surface defects and recombination sites, leading to improved device stability and efficiency.

Despite the potential to resolve the high-temperature processing limitations, ZnO-based PSCs remain vulnerable to substantial long-term stability problems, primarily due to UV degradation.[122] The stronger UV catalytic activity of ZnO leads to severe degradation issues, than TiO_2. Surface hydroxyl groups and residual chemicals on the solution-processed ZnO surface induce photochemical reactions under UV exposure, accelerating the decomposition of the light-harvesting layer. This degradation mechanism critically undermines the stability and efficiency of ZnO-based PSCs, highlighting the urgent need for strategies to enhance their UV resistance. The interaction between ZnO and metal halide perovskites results in the chemical instability of ZnO, which triggers a swift deterioration of the perovskite layer.[123] This instability hinders the potential use of ZnO as an n-type charge extraction layer in high-performance PSCs, despite its superior optoelectronic properties compared to other MOs like SnO_2 and TiO_2.

3.1.3 Tin oxide (SnO_2). The predominant challenge associated with MOs, such as TiO_2 and ZnO, is their interaction with ultraviolet (UV) light. Under UV irradiation, these materials function as photocatalysts, thereby enhancing the degradation process of perovskite materials. This degradation process is initiated when UV light excites electrons within TiO_2, leading to the creation of deep-level defects and augmented interface carrier recombination. These phenomena collectively result in a substantial diminution of PSC performance. Typically, SnO_2 is recognized for its excellent UV light absorbance due to its wide band gap, which makes it an effective photocatalyst under UV radiation.[124,125] SnO_2 being chemically inert with negligible catalytic performance, and its larger BG compared

Table 2 Photovoltaic features of TiO_2, SnO_2, and ZnO[112–121]

	TiO_2	ZnO	SnO_2
Energy band gap (eV)	3.0–3.2	3.2–3.3	3.50–4.0
Electron mobility ($cm^2\ V^{-1}\ s^{-1}$)	20	2.05×10^2	10^{-8}–10^2
Efficiency% (η)	20–25	19–21.90	23–26
Surface work function (eV)	4.5–5.0	4.45–5.3	4.71–5.3
Electron diffusion coefficient ($cm^2\ s^{-1}$)	0.5–10^{-8}	5.2–1.7×10^{-4}	6.22×10^{-6}

to TiO_2 makes it less susceptible to these issues. SnO_2 UV resistance and lower photocatalytic activity contribute to its ability to maintain device stability and lifespan under UV exposure, providing a more stable alternative as an ETM in PSCs. Additionally, SnO_2 boosts significantly higher electron mobility, up to 240×10^{-4} cm^2 V^{-1} s^{-1}, compared to TiO_2 (10^{-4} cm^2 V^{-1} s^{-1}) (Table 1).[126] This higher electron mobility facilitates more efficient electron collection and transport, directly contributing to improved device performance. Furthermore, the reduced hygroscopic nature and enhanced resistance to acidic conditions of SnO_2 contribute to its longevity, resulting in solar cells with extended operational lifespans. The fabrication process of SnO_2 also presents significant advantages. SnO_2 can be synthesized at low temperatures (<180 °C), in contrast to the high-temperature processes often required for TiO_2. The nanocrystalline SnO_2, processed through low-temperature solution methods, can effectively function as a viable substitute for TiO_2 as an ETM. A wide range of electron mobility values for SnO_2 (from 10^{-8} to 10^2 cm^2 V^{-1} s^{-1}) has been reported (Table 2), which can be primarily attributed to variations in synthesis methods, crystallinity, and defect concentrations. Factors such as oxygen vacancy density, grain boundary scattering, and surface roughness critically influence charge transport. Films prepared *via* low-temperature or solution-based processes often exhibit poor crystallinity and high defect densities, leading to reduced mobility. In contrast, high-temperature or vacuum-based techniques generally produce well-ordered structures with significantly improved mobility.[127] Furthermore, SnO_2 offers excellent band alignment with light-harvesting layers, which is crucial for efficient electron transfer and minimizing energy losses.[128] This favorable CB alignment helps form high-quality p–n heterojunctions, reducing charge recombination and thereby improving the V_{oc} and FF of the PSCs. The ability of SnO_2 to serve both as a compact layer and a mesoporous layer adds to its versatility, allowing for more flexible design and optimization of PSC architecture. This versatility is instrumental in achieving higher efficiencies and developing more robust and scalable solar cell designs. However, SnO_2 as an ETM in PSCs faces challenges, including the need for dense, pinhole-free films, as pinholes can reduce efficiency. Low-temperature annealing can cause defects, increasing charge carrier recombination and reducing device performance. Additionally, SnO_2 films often require surface treatments, like UV-ozone, to remove residues and improve wettability, adding complexity to the manufacturing process. The intricate surface characteristics inherent to TMOs, notably including oxygen vacancies, ionic residues, and suspended bonds, introduce supplementary non-emissive recombination sites. Consequently, these phenomena exert adverse effects on the crystallization and interfacial contact of the light-harvesting layer, thereby impeding device performance and stability. Moreover, the disparate carrier mobility and limited conductivity exhibited by ETMs and HTLs contribute to the accumulation of carriers at interfaces and consequent resistance losses. These challenges exacerbate hysteresis effects and promote charge recombination within the device structure.[129]

3.2 Organic ETMs

The limitations of metal oxide-based ETMs, particularly their high processing temperatures and incompatibility with flexible substrates, have driven significant interest in organic alternatives. Organic ETMs offer distinct advantages, including solution processability, tunable electronic properties, and compatibility with roll-to-roll (R2R) fabrication, making them indispensable for scalable and flexible perovskite photovoltaics.[130] Among these, fullerene derivatives (*e.g.*, C_{60}, PCBM) have emerged as leading candidates due to their exceptional electron affinity and ability to passivate interfacial defects, enabling PCEs exceeding 22% in optimized devices.[131,132]

Despite their advantages in processing versatility and interfacial engineering, organic ETMs face intrinsic limitations that constrain their widespread adoption in PSCs,[133] such as lower electron mobility (<10^{-2} cm^2 V^{-1} s^{-1}) compared to inorganic ETMs (*e.g.*, SnO_2, TiO_2), leading to resistive losses in thick-film devices.[134] Furthermore, interfacial energy disorder at perovskite/ETM junctions exacerbating non-radiative recombination losses, while the thermodynamic instability of carbon-based molecular frameworks under operational stressors (photo-oxidation, thermal degradation) poses fundamental challenges for long-term device viability.[32] These material-level constraints underscore the need for innovative molecular design strategies that reconcile electronic performance with environmental robustness to unlock the full potential of organic ETMs in commercial PSC architectures.

4. Exploring the charge dynamics of fullerenes and fullerene derivatives in PSCs

Fullerenes and their derivatives are pivotal in PSCs due to their high electron affinity, tunable energy levels, and defect passivation capabilities. This section examines how pristine and functionalized fullerenes optimize photocarrier dynamics, charge generation, separation, transport, and recombination, and highlights recent spectroscopic insights into their molecular-level contributions.

4.1 Pristine fullerene

While n-type metal oxides have traditionally dominated as ETMs in conventional PSCs, their practical implementation faces significant limitations. These include suboptimal film quality, oxygen vacancy-induced defect states, inherent chemical instability, and pronounced hysteresis effects, all of which collectively constrain device performance metrics. In contrast, pristine fullerenes (C_{60} and C_{70}), serve as effective ETMs due to their LUMO levels (~3.7–4.0 eV), which align well with perovskite conduction bands.[30] Their icosahedral structure enables efficient electron extraction, reducing recombination losses. For example, C_{60}-based PSCs achieve PCEs of 20–23%.[135] However, their hydrophobicity and tendency to aggregate limit

film uniformity, increasing trap states and reducing carrier diffusion lengths (<100 nm).[136]

4.2 Fullerene derivatives

The optimization of photocarrier dynamics in perovskite solar cells necessitates the strategic functionalization of fullerene derivatives (Fig. 4a),[7] as the implementation of pristine fullerenes as ETM presents significant limitations. Poor solubility in common organic solvents (chlorobenzene, chloroform), restricting processing window. Non-uniform films with incomplete surface coverage (<80%), leading to inconsistent charge transport pathways. This morphological imperfection creates inconsistent charge transport pathways and compromises interfacial contact with the perovskite layer, ultimately manifesting as increased series resistance exceeding 10 Ω cm^2 and elevated trap-assisted recombination with carrier lifetimes shorter than 20 ns.[9,129] Functionalized fullerenes, such as PCBM, are limited by issues including photochemical instability, high cost, and restricted tunability.[31] In contrast, non-fullerene ETMs offer enhanced structural diversity, tunable electronic properties, and improved film morphology.[137] For example, perylene diimides (PDIs) and naphthalene diimides (NDIs) have demonstrated comparable or even superior device performance with enhanced long-term stability, achieving PCEs of up to ~20.5%. Moreover, polymer-based ETMs such as P(NDI2DT-TTCN) and PFN-2TNDI exhibit excellent processability, thermal stability, and competitive efficiencies ranging from ~17% to 20.8%. Additionally, oxygen-doped graphitic carbon nitride has been shown to enhance ETM performance in PSCs by passivating interfacial trap states and improving energy level alignment. This results in reduced charge recombination, improved charge extraction, and PCEs exceeding 21%, along with enhanced device stability. Nonetheless, challenges persist in achieving consistently high charge mobility and scalable fabrication.[31]

This review systematically examines key classes of fullerene derivatives (Fig. 4b), focusing on their role in optimizing charge dynamics in PSCs. Notably, functionalized fullerenes such as PCBM and 5F-PCBP (Fig. 4c) effectively passivate iodine vacancies at perovskite interfaces, thereby enhancing charge extraction efficiency. Further modifications, including hydrophilic variants (–OH, –COOH, $–NH_2$), improve both solution processability and interfacial charge extraction, addressing critical limitations of pristine fullerenes.[7] Lewis acidic derivatives effectively modify cathode work functions for better energy alignment. Halogenated fullerenes demonstrate increased electron affinity, benefiting open-circuit voltage.[140] Oligoethylene glycol and crown ether modifications significantly broaden solvent compatibility. Pyridine/thiophene-functionalized derivatives excel in defect passivation through Pb^{2+} coordination (Fig. 4d). Cross-linked versions create robust, thermally stable charge transport networks. Notably, ICBA and

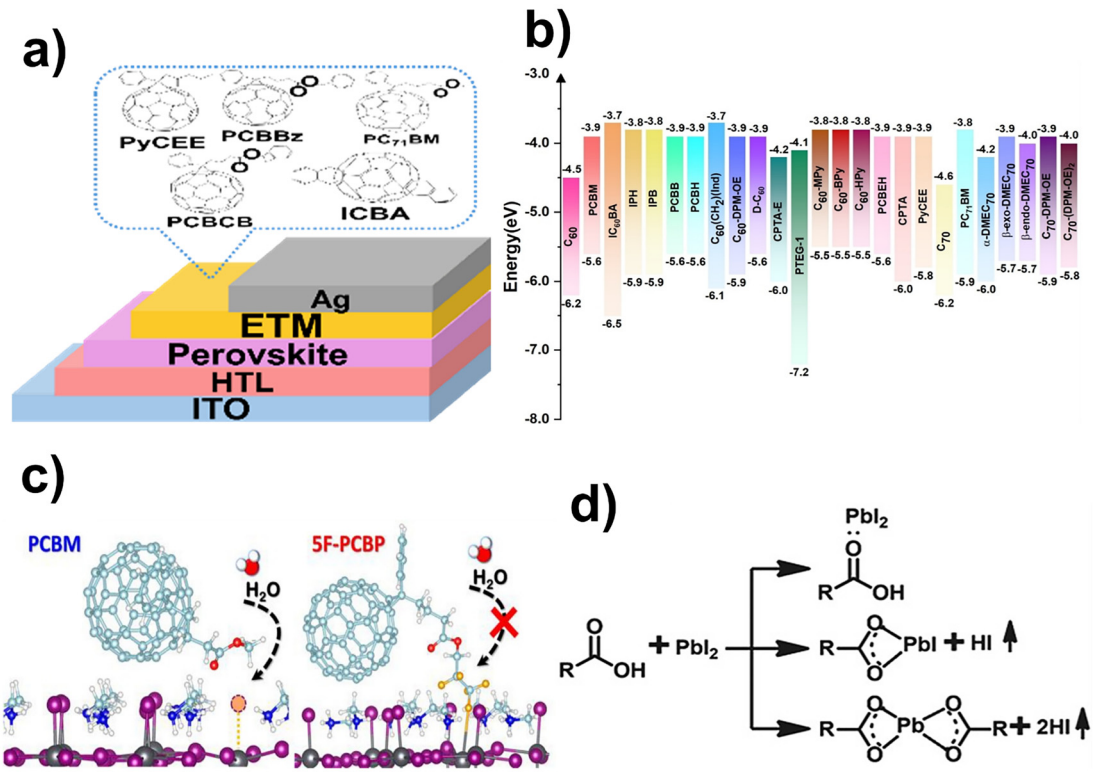

Fig. 4 (a) The structural design of fullerene derivatives and illustration of the planar PSC, (b) energy level diagram of various functionalized fullerenes in PSCs,[30] (c) the interface between the perovskite/PCBM and perovskite/5F-PCBP layers reveals the presence of iodine vacancies on the perovskite surface,[138] and (d) proposed pathways for the formation of CPTA : PbI_2 complexes.[139]

its analogues with elevated LUMO levels have proven particularly effective for achieving higher photovoltages.[141] Each derivative class offers distinct advantages for addressing specific challenges in charge carrier management, as will be explored in subsequent sections. This strategic functionalization enables precise tuning of electronic properties, interfacial interactions, and morphological stability in PSC architectures.

4.3 Hydrophilic fullerene

The intrinsic hydrophobicity of pristine fullerenes poses substantial challenges for their effective integration into perovskite solar cell architectures, particularly in solution-processed fabrication methods.[136] This limitation stems from strong π–π stacking interactions that promote aggregation and poor interfacial compatibility with polar components in the device stack. To address these constraints, researchers have developed three principal strategies to enhance hydrophilicity and processability. The first approach involves the formation of stable colloidal aggregates through carefully controlled solvent exchange processes, where extended sonication aids in achieving uniform dispersion. A second pathway utilizes non-covalent modification techniques that leverage hydrogen bonding networks, π–π stacking interactions, or electrostatic stabilization to improve aqueous compatibility without altering the core fullerene structure. Notably, covalent functionalization with hydrophilic moieties (–OH, –COOH, $–NH_2$ groups) has emerged as the most versatile solution, (Fig. 5a). These chemical modifications not only dramatically improve solubility in polar media but also introduce beneficial interfacial properties that enhance charge extraction while maintaining the essential electronic characteristics of the fullerene core.

The C_{60}'s icosahedral symmetry limits functionalization to specific carbon atoms, affecting the degree of modification. Wang *et al.* demonstrated this principle by developing 5F-PCBP, a fluorinated PCBM derivative, which achieved a remarkable PCE of 21.27% in triple-cation PSCs, (Fig. 4).[144] The fluorinated ETM exhibited exceptional stability, with encapsulated devices showing a projected T_{80} lifetime exceeding 92700 hours (~10 years) under operational conditions. This performance enhancement stems from the synergistic effects of fluorination: increased surface hydrophobicity, suppression of iodine vacancies, and stabilization of organic cations at the perovskite interface.

Alternative modification strategies have explored polar functional groups to optimize interfacial properties. Wang and colleagues investigated CPTA-E (Fig. 5b), a fulleropyrrolidine derivative featuring three carboxylic ester groups, as a PCBM alternative in p–i–n PSCs (Fig. 5(c and d)).[33] While CPTA-E shows reduced solubility in chlorobenzene compared to PCBM, solvent blending with chloroform enabled effective processing. More critically, the carbonyl groups in CPTA-E strongly coordinate with undercoordinated Pb^{2+} ions at the perovskite surface, forming a uniform passivation layer that reduces interfacial recombination. This molecular design yielded devices with 17.44% PCE and minimal hysteresis, outperforming PCBM-based control devices (15.09% PCE with pronounced hysteresis). Cross-sectional SEM analysis (Fig. 5e) confirmed the improved morphology and interfacial integrity achieved with CPTA-E.

These case studies illustrate how targeted functionalization of fullerenes can simultaneously address multiple challenges in PSCs, enhancing solubility, improving interfacial charge extraction, and boosting device stability through carefully engineered molecular interactions at the perovskite/ETM interface, (Fig. 5f).

4.4 PCBM-based fullerene derivatives

The ELA between $MAPbI_3$ perovskites and fullerene derivatives presents both opportunities and challenges for charge carrier

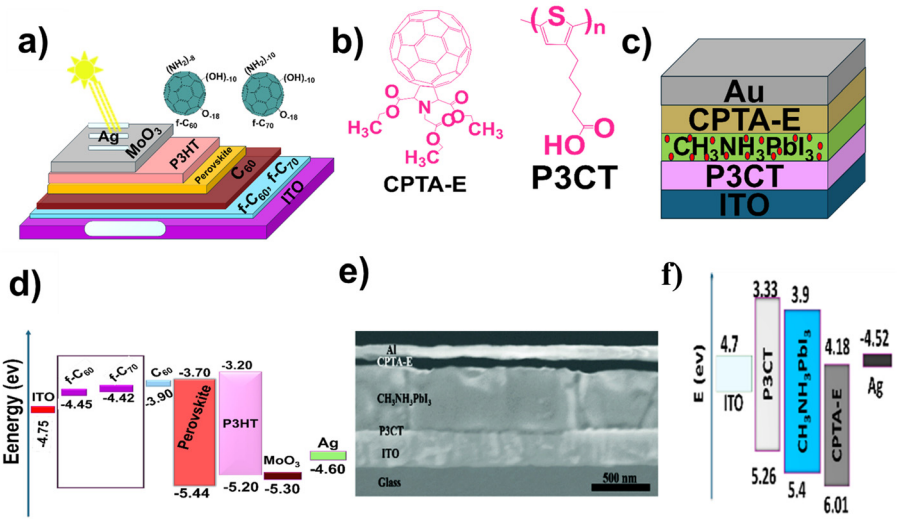

Fig. 5 (a) Schematic diagram of hydrophilic fullerene,[142] (b) the chemical configurations of CPTA-E and P3CT, (c) a schematic depiction of the p–i–n structured PSC device employing CPTA-E as the ETM along with its corresponding (d) energy level diagram, (e) SEM image showing a cross-section of the device, and (f) energy level diagram for each layer is shown correspondingly.[143]

management. While the 0.7 eV ΔE between the $MAPbI_3$ valence band and C_{60}'s HOMO level provides adequate hole-blocking capability, this configuration is not optimal for maximizing device efficiency. This ΔE creates conditions where photogenerated holes may transfer to adjacent C_{60} molecules, leading to interfacial recombination losses. PCBM exacerbates this issue further, with a reduced 0.4 eV valence band offset between the perovskite valence band and the HOMO level (compared to C_{60}) further compromises hole-blocking efficiency. This limitation necessitates the implementation of additional interfacial layers to optimize charge extraction dynamics.[145]

A more fundamental challenge arises from defect states (DSs) associated with perovskite crystallinity, particularly at grain boundaries (GBs) and CTL interfaces. These structural imperfections act as trapping centers for charge carriers before they reach the electrodes. Fullerenes mitigate these defects through two primary passivation mechanisms: (1) physical passivation by filling GB voids *via* large molecular size, and (2) chemical passivation through coordinating undercoordinated Pb^{2+}/I^- ions, as well as electronic passivation by delocalized π-electrons quench trap states. However, PCBM's tendency to form large aggregates during deposition reduces interfacial contact area, and its photodimerization under illumination significantly degrades charge transport properties.[146] Recent advances in evaporable fullerene derivatives, such as the fullerene indanones (FIDOs) developed by Shui *et al.*, have addressed these limitations. FIDO-based devices achieved a remarkable 22.11% PCE compared to 18.2% for conventional C_{60} devices, though long-term stability remains a concern.[147]

Meng and colleagues systematically investigated the structure–property relationships of PCBEH (Fig. 6a), a PCBM analogue functionalized with branched alkyl chains, demonstrating significant improvements in both device performance and stability.[7] Their study, employing dynamic light scattering (DLS) and solution-state NMR, confirmed PCBEH's superior chlorobenzene solubility (~52 mg mL^{-1}) *vs.* PCBM (~35 mg mL^{-1}), enabling the formation of exceptionally uniform thin films with enhanced interfacial properties. This improved morphology directly correlated with more effective defect passivation and optimized electron extraction dynamics, ultimately yielding champion devices with power conversion efficiencies reaching 16.26% – a notable improvement over standard PCBM-based architectures.[144]

The branched alkyl functionality of PCBEH contributed to two key advantages: first, the enhanced hydrophobicity (contact angle of 97° *versus* PCBM's 81°) provided superior moisture resistance, and second, the optimized molecular packing reduced interfacial trap states.[150]

Atomic force microscopy characterization (Fig. 6b) provided quantitative insights into the morphological improvements, showing that PCBEH deposition on perovskite substrates reduced the root-mean-square surface roughness from 54 nm (bare perovskite) to 13.7 nm, outperforming PCBM's smoothing effect to 19.3 nm (Fig. 6c). This dramatic reduction in surface roughness reflects PCBEH's ability to more effectively template the perovskite interface, minimizing contact imperfections that typically promote non-radiative recombination. The combination of enhanced solution processability, improved interfacial morphology, and intrinsic hydrophobicity positions alkyl-functionalized fullerene derivatives like PCBEH as promising candidates for developing high-performance as well as environmentally stable perovskite photovoltaics. These findings underscore the critical importance of side-chain engineering in tailoring fullerene derivatives for specific interfacial challenges in PSC architectures.[151]

4.5 [6,6]-Phenyl-C61-butyric acid benzyl ester (PCBB)

To overcome PCBM's photoinduced aggregation, Wang *et al.* developed PCBB, a structural analogue where the terminal methyl group is replaced with a benzyl moiety.[33] This strategic modification significantly enhances molecular stability and retain >80% initial PCE after 600 hours at maximum power point, achieves 19.84% PCE (Table 3), a marked improvement over conventional PCBM-based systems. This enhanced performance stems from two key molecular interactions: (1) strengthened π–π stacking between C_{60} cages that maintains electron delocalization, and (2) CH–π bonding between benzyl groups that provides steric stabilization. Together, these interactions effectively suppress fullerene aggregation – a critical advancement over conventional PCBM systems. Recent studies by Zhang *et al.* have further confirmed that such aromatic substitutions in fullerene derivatives reduce trap state formation at perovskite interfaces (Fig. 7a), explaining the observed enhancement in both efficiency and operational stability.[152] This molecular design approach (Fig. 7b) offers a promising pathway to overcome one of PCBM's most persistent limitations in PSC applications.

4.6 Lewis base functionalized fullerene derivatives

Functionalizing fullerenes with Lewis base groups (amines, oligoethers, crown ethers) improves their performance as ETMs by simultaneously enhancing polarity (enabling better processing), defect passivation (*via* Pb^{2+} coordination), and ELA at perovskite interfaces.[167] These modifications strengthen interactions with ionic species in perovskites, reducing recombination while maintaining charge transport efficiency, a key advancement beyond conventional ester/alkyl modifications.

4.6.1 Amino-functionalized fullerene derivatives. Amino groups, including $-NH_2$ and $-N^+(CH_3)_3I^-$, serve as effective Lewis bases for fullerene functionalization, creating dipole-induced fields that enhance charge collection through dipole-induced built-in electric fields.[138] These modifications simultaneously passivate defects and modify interfacial energy bands. Xiang *et al.* demonstrated the dual functionality of $C_{60}NH_2$ by employing it as a modifier for the TiO_2 ETM in planar n–i–p PSCs, achieving a PCE of 18.34%. The enhanced performance was attributed to reduced hysteresis resulting from improved electronic coupling at the perovskite/TiO_2 interface and lattice stabilization.[168]

Further advancements emerged from Li *et al.*'s PCBB-S-N (Fig. 10d), combining thiophene and amino groups into an

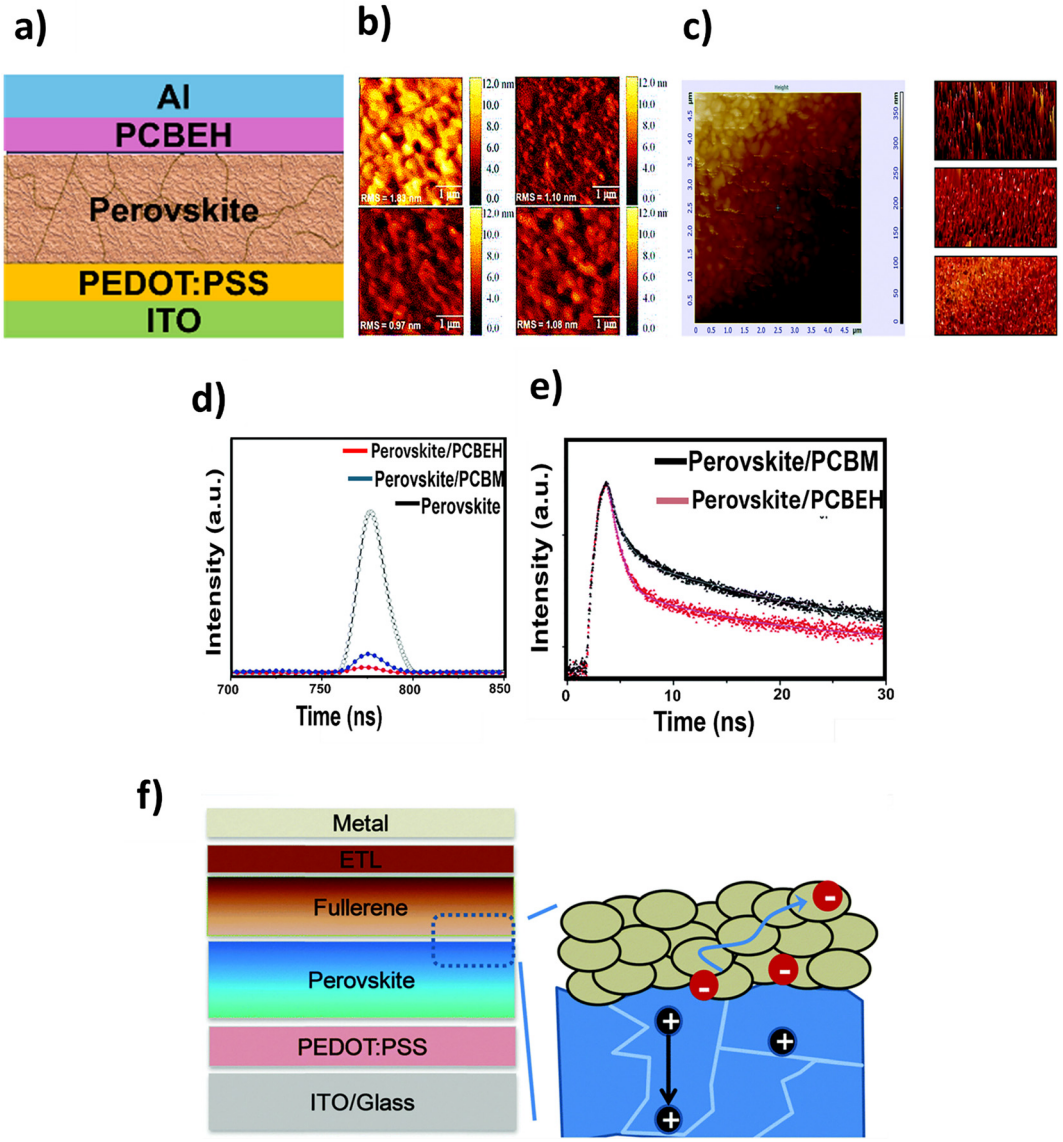

Fig. 6 (a) An illustration of PCBEH-based PSC.[148] (b) AFM images for the perovskite/PCBM : C_{60} configuration, highlighting various volume ratios of PCBM : C_{60}, (c) the PL and TRPL decay transient spectra of the FTO/perovskite/PCBM (or PCBEH),[149] (d) a schematic representation of the layer configuration of fullerene-based PSCs, with and without the application of PCBB-3N-3I, (e) chemical structures of FDs, and (f) Charge transfer mechanism on perovskite films.[143]

interlayer that reached 21.08% PCE. The thiophene moiety coordinated with Pb^{2+} ions while the amino group formed hydrogen bonds, producing dense PCBM films and optimized energy band alignment. Zhang *et al.* extended this approach with PCBB-3N-3I, where coulombic interactions with charged defects yielded 21.1% PCE and enhanced stability through defect neutralization and dipole layer formation.[169] For inverted architectures, PCBDMAM interlayer boosted PCE from 14.21% to 18.10% by reducing the Ag cathode work function and minimizing interfacial barriers between PCBM and electrodes.[170]

4.6.2 Oligoether and crown-ether functionalized fullerene. The exploration of polar Lewis bases beyond amino groups has opened new avenues for fullerene-based ETMs, with crown ether (CE) and oligoether (OE) functionalizations demonstrating particular promise. This development builds on earlier work with amino groups, extending the toolkit for interfacial engineering in PSCs. Chen *et al.* pioneered this approach by developing bis-C_{60} as a cathode buffer layer (CBL), where its unique structure improved ELA between PCBM and Ag electrodes, achieving 11.8% PCE.[171]

This advanced designs inspired subsequent innovations, such as Voroshazi *et al.* bis-FIMG and bis-FITG CBLs, which reached ~19% PCE by combining the conductivity advantages of fullerene derivatives with improved work function modulation.[172]

Table 3 presents the photovoltaic characteristics of devices incorporating various functional additives based on fullerenes[104,107,112,138,143,144,150,156–166]

Compounds	LUMO/eV	μ ($cm^2\ V^{-1}\ s^{-1}$)	FF/%	PCE%
PCBM	−3.70	—	58.37	21–23
PCBB	−3.90	3.09×10^{-4}	80.39	19.84
PCBA	−4.2	—	72	17.76
CPTA	−3.9	5.4×10^{-3}	75.61	18.39
Sol–gel C_{60}	−3.85	3.8×10^{-4}	73	17.9
PCBCB	−3.8	5.9×10^{-3}	73	17.9
$MPMIC_{60}$	−4.1	—	64	13.8
PCBC	—	—	81	15.71
C_{60}-MPy	−3.80	1.97×10^{-3}	78.4	16.1
CPTA	−3.9	5.4×10^{-3}	75.61	18.39
ICBA	−3.74	3×10^{-3}	79	23.8
ICTA	−3.36	—	74.2	18.04
ICMA	−3.85	—	64.7	13.9
CPTA-E	−4.18	3.8×10^{-4}	80	17.44
C_{60}-MPy	−3.80	1.97×10^{-3}	78.4	16.1
C_{60}-HPy	−3.83	1.04×10^{-3}	70.8	14.4
C_{60}-BPy	−3.81	3.51×10^{-3}	74.2	18.22
PCP	−3.81	2.64×10^{-3}	78	19.32
P_yCEE	−3.94	5.76	75.83	18.27
PCBBz	−3.80	3.70×10^{-4}	69	16.57
PCBH	−3.90	—	79	13.75

The relationship between molecular structure and device performance becomes particularly evident in Cao *et al.*'s systematic study of OE-functionalized fullerenes. Their optimized C70-DPM-OE derivative, featuring electron-rich OE chains, not only enhanced interfacial charge mobility but also effectively passivated defects, yielding 16% PCE.[173] This success highlights how tailored functional groups can address multiple device challenges simultaneously. Further insights into molecular interactions emerged from comparative studies of different Lewis base functionalities. MCM (OE-functionalized) and PCP (pyridine-functionalized) derivatives (Fig. 7d) revealed a crucial structure–property relationship: while the stronger N–Pb^{2+} coordination in PCP improved interfacial contact, it also introduced energetic misalignment that exacerbated hysteresis. The crown-ether approach developed by Liu *et al.* with PCBC demonstrated how molecular engineering can improve interfacial physics. By serving as an effective CBL between PCBM and aluminum electrodes, PCBC enhanced ohmic contact and electron extraction, achieving 15.08% PCE. The subsequent development of PCBC/LiF bilayers further improved performance (15.53% PCE), illustrating the cumulative benefits of layered interfacial engineering.

Parallel developments in PEG-functionalized fullerenes addressed the critical challenge of device stability. Zhu *et al.* showed that increasing PEG moieties enhanced moisture resistance, while Xie *et al.* demonstrated how PEG-capped derivatives could simultaneously improve crystallinity, reduce defects, and enhance charge transfer, with PCEs consistently around 17.7%.[174,175] These studies collectively established PEG-functionalization as a versatile strategy for stability enhancement.

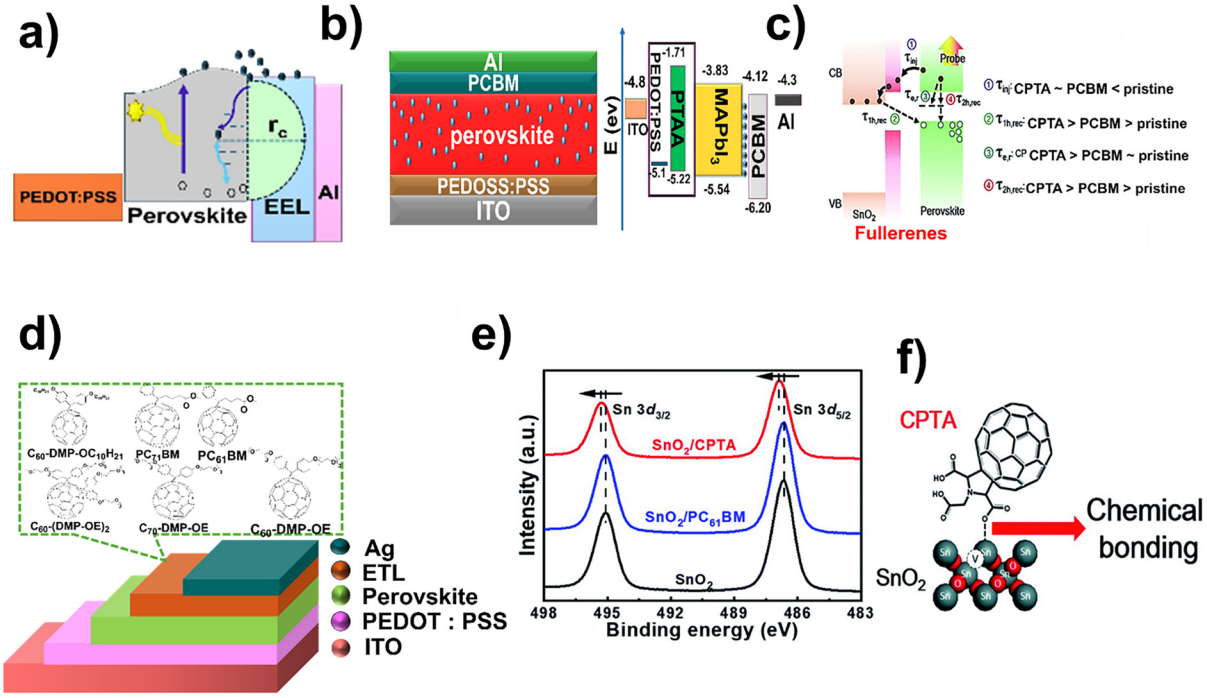

Fig. 7 (a) Suggested framework for the light-soaking effect,[153] (b) the architectural design of devices utilizing PSCs, encompasses the chemical compositions and energy states of various fullerene derivatives, (c) device architecture and their corresponding energy states diagram of the PSCs,[154] (d) the physical adhesion between the SnO_2 surface and PC61BM. Panel (e) displays high-resolution XPS spectra of the Sn 3d core level for SnO_2, SnO_2/PC61BM, and SnO_2/CPTA films, and (f) the chemical bond formation between the SnO_2 surface and CPTA.[155]

The critical role of chemical bonding mechanisms was conclusively demonstrated by Huang *et al.*'s comparison of CPTA and PCBM on SnO_2 surfaces (Fig. 7(c and e)). The strong chemical bonding of CPTA's carboxyl groups created beneficial interfacial dipoles (Fig. 7f), reducing recombination and achieving 19% PCE – significantly outperforming PCBM's physisorption approach (17.9% PCE) and unmodified SnO_2 (16.4% PCE). This work provided fundamental insights into passivation mechanisms while showcasing the performance potential of properly designed fullerene derivatives.[155]

4.6.3 Heterocyclic pyridine and thiophene functionalized fullerene derivatives. The electronic properties of fullerene-based ETMs can be precisely tuned through strategic incorporation of π-conjugated heterocycles like pyridine and thiophene (Fig. 8a).[33] These aromatic modifications serve dual rules: they optimize π–π stacking interactions between fullerene cages while introducing coordination sites for perovskite defect passivation. The curved geometry of C_{60} provides an ideal platform for these functionalizations, where conjugated systems enhance charge transport and flexible side chains prevent aggregation without compromising solubility, a critical balance for high-performance ETMs.

Xing *et al.* established a design paradigm for these materials through systematic development of pyrrolidine-based derivatives (C_{60}-HPy, C_{60}-BPy, C_{60}-MPy) (Fig. 8b).[177] Their work revealed two key structure–function relationships: (1) longer *N*-alkyl chains improve moisture resistance by encapsulating the perovskite layer, while (2) pyridine-Pb^{2+} coordination directly reduces interfacial defects (Fig. 8c). This understanding enabled Cates group to develop C_{60}-3-Py, where *meta*-positioned nitrogen sites achieved 17.57% PCE in $MAPbI_3$ devices through enhanced defect passivation.[178] The superiority of pyridine-functionalized ETMs becomes evident in comparative studies with conventional materials. Vasilopoulou *et al.* PCBBz demonstrated advantages over TiO_2 across multiple parameters, higher charge mobility, enhanced ELA, and improved wetting properties, culminating in 18.27% PCE.[179] These findings were extended to mixed-cation devices by Wang Ye, where C_{60}-3-BPy achieved 18.22% PCE in CsFAMA PSCs *versus* 15.70% for PCBM controls, attributed to improved

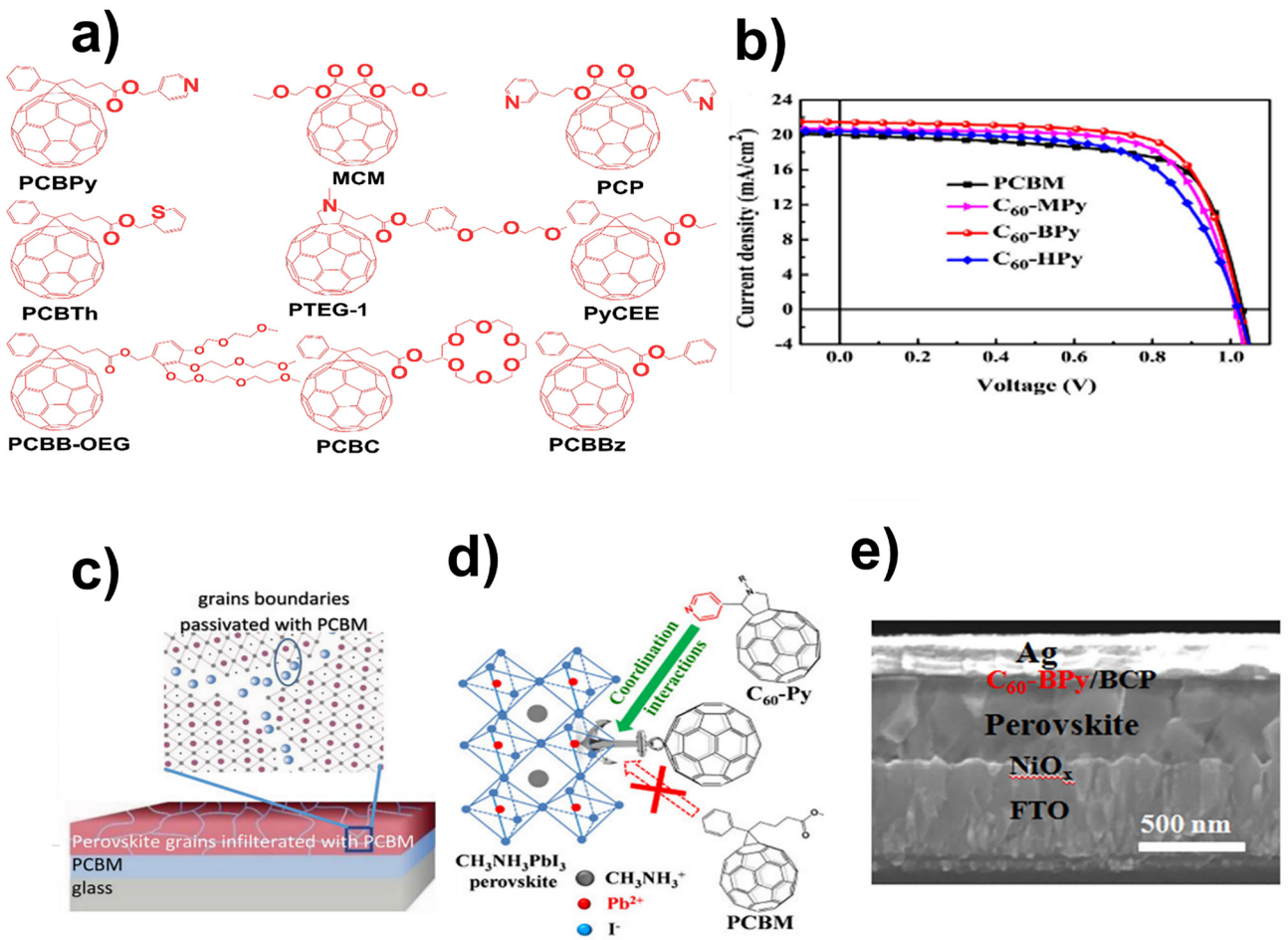

Fig. 8 (a) The molecular configurations of heterocyclic functionalized fullerene utilized in PSCs,[157] (b) *J*–*V* profiles of the control and C_{60}-Py ETM-based device, (c) the device structure indicates the diffusion of PCBM molecules through the grain boundaries of the perovskite layer,[22] (d) schematic demonstration of interaction between light-harvesting layer and fullerene ETMs,[176] and (e) SEM image of a device incorporating C_{60}-BPy as ETM.

energy level modulation and perovskite crystallization.[180] Zhu *et al.*'s work with C_{60}-BPy, Sn-based PSCs highlighted the versatility of this approach (Fig. 8d). The strong Sn-pyridine interaction reduced surface trap density while optimizing energy alignment, yielding 14.14% PCE with exceptional light-soaking stability (95% retention after 1000 hours).[181] This demonstrates how molecular modifications address both efficiency and stability challenges, a critical requirement for commercial viability (Fig. 8e). As summarized in Table 3, these rationally designed derivatives outperform conventional fullerenes across multiple performance metrics while offering processing advantages. Their development represents a significant step toward tailored interfacial materials that can address the complex requirements of high-efficiency, stable PSCs.

A functionalized fullerene derivative, C_{60}-BPy, has shown promise in enhancing Sn-based PSCs by improving electron extraction, reducing interfacial recombination, and enhancing ELA.[182] Its integration also improves film quality and device stability (Fig. 9a). In a subsequent development in 2024, Sun and colleagues developed another novel pyridine-functionalized fullerene derivative, PyCEE, which was employed as an alternative to the conventional TiO_2 ETM in planar n–i–p PSCs (Fig. 9(b and c)). Compared to TiO_2, the PyCEE ETM exhibits a less wettable surface, more favorable energy level alignment, higher electron mobility, and enhanced trap passivation through coordination interactions with Pb^{2+} ions in the $CH_3NH_3PbI_3$ film.[183] These properties facilitate the formation of large-grained perovskite films, improve electron extraction and transport, reduce hysteresis, and yield a champion PCE of 18.27%.[179] Beyond their use as ETMs in PSCs, the integration of heterocyclic pyridine- and thiophene-functionalized fullerene derivatives as additives within the perovskite layer offers an effective strategy for enhancing the performance of bulk heterojunction (BHJ) PSCs. In 2020, Lingbo Jia and his group developed a pyridine-functionalized fullerene derivative, C_{60}-PyP,[157] and incorporated it as an additive in the $CH_3NH_3PbI_3$

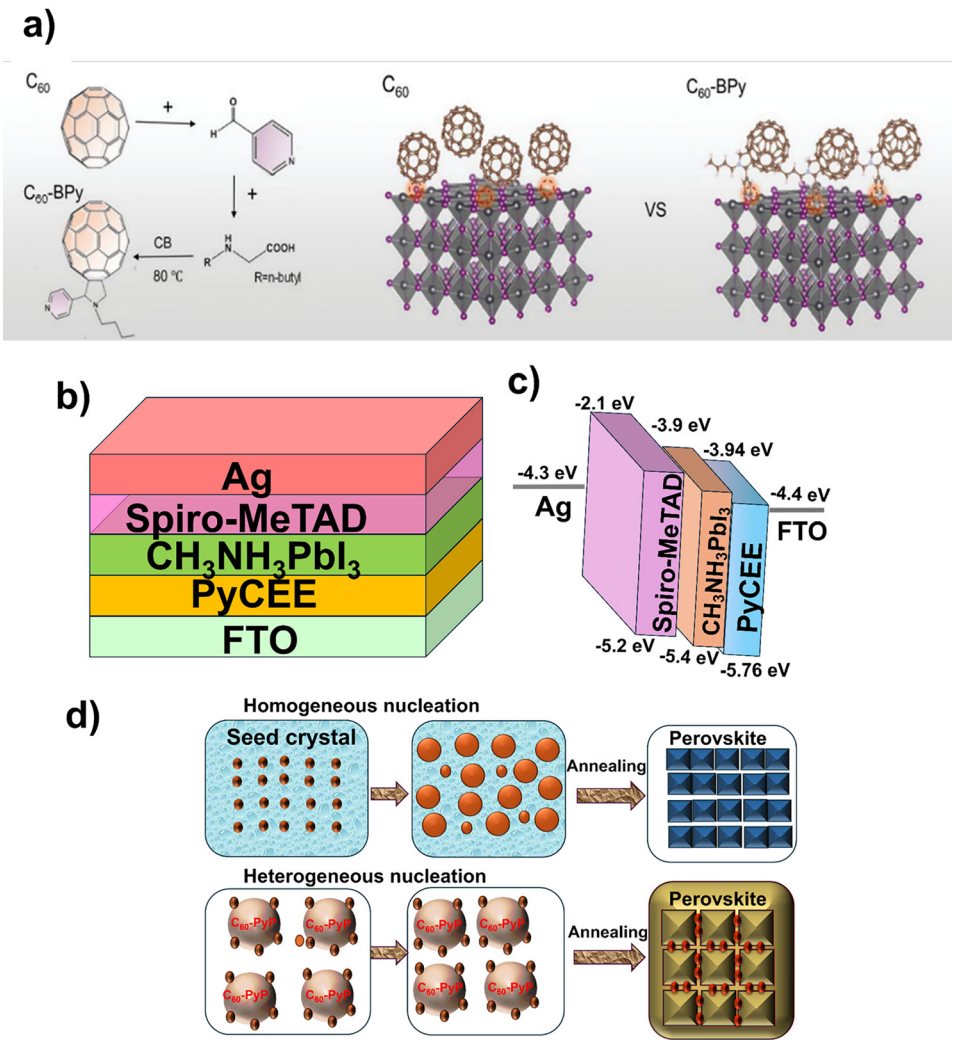

Fig. 9 (a) The structure of C_{60}-BPy and its schematic representation illustrate the interfacial interactions between the perovskite layer and C_{60}-BPy,[181] (b and c) device structure of PyCEE and energy level diagram, and (d) diagrammatic representation of perovskite nucleation with and without C_{60}-PyP.[184]

perovskite film of p–i–n PSCs. The addition of C_{60}-PyP reduced the nucleation Gibbs free energy and promoted controlled crystalline orientation, leading to enhanced crystallinity and a significant reduction in trap states (Fig. 9d).[184] This improvement stemmed from the coordination interaction between the nitrogen atom of the pyridine group and Pb^{2+} ions in the perovskite. Consequently, the optimized devices achieved a champion PCE of 19.82%, a substantial enhancement compared to control devices without the additive.

4.7 Fullerene derivatives with carboxyl and hydroxyl groups

4.7.1 Carboxyl functionalized fullerene derivatives/carboxylate (COOH) fullerene derivatives. The inherent limitations of MO ETMs in planar PSCs, particularly oxygen vacancy-related defects that hinder charge transport, have spurred the development of carboxyl-functionalized fullerene derivatives as interfacial modifiers, (Fig. 10a). These materials address two critical challenges simultaneously: passivating surface defects while optimizing ELA (Fig. 11a). Roy *et al.* pioneered this approach with C_{60}-SAM, a carboxylated fullerene self-assembled monolayer that reduced trap-assisted recombination at TiO_2 interfaces, achieving 17.3% PCE in mixed-halide perovskites with minimal hysteresis.[185] The success of this strategy stems from the dual functionality of carboxyl groups anchoring firmly to metal oxide surfaces while passivating perovskite defects through coordination with Pb^{2+} ions. This concept has been expanded through various molecular designs. Mora-Seró's cyano-carboxyl fullerene derivatives demonstrated how combining multiple functional

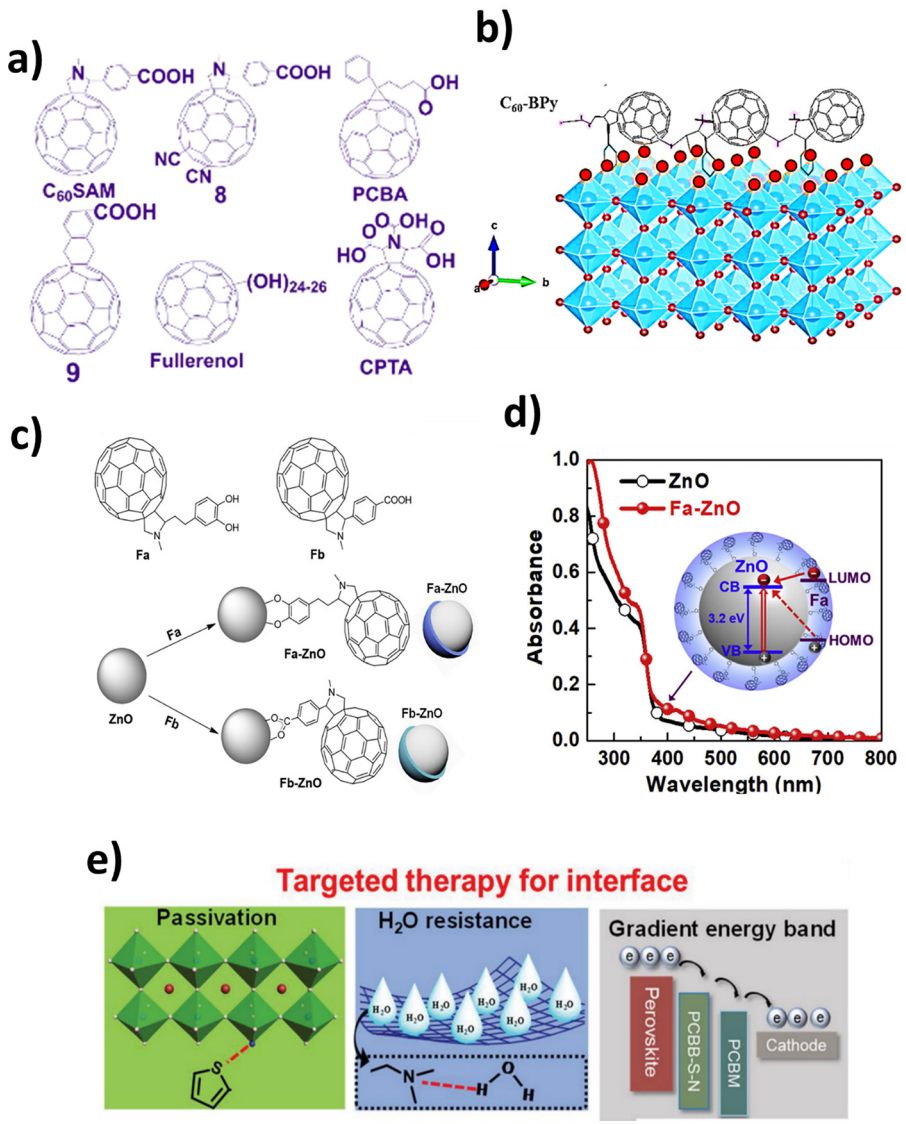

Fig. 10 (a) The molecular architectures of functionalized fullerene featuring carboxyl and hydroxyl groups, which are applied in PSCs,[157] (b) the illustration depicting the interaction between perovskite materials and fullerene derivatives,[138] (c) schematic demonstration that details the coating of fullerene derivatives on ZnO nanoparticles characterized by core–shell configurations, (d) an illustration of the functions of PCBB-S-N,[186] and (e) analysis of the UV-visible absorption spectra of the pertinent films characterized by core–shell configurations.[187]

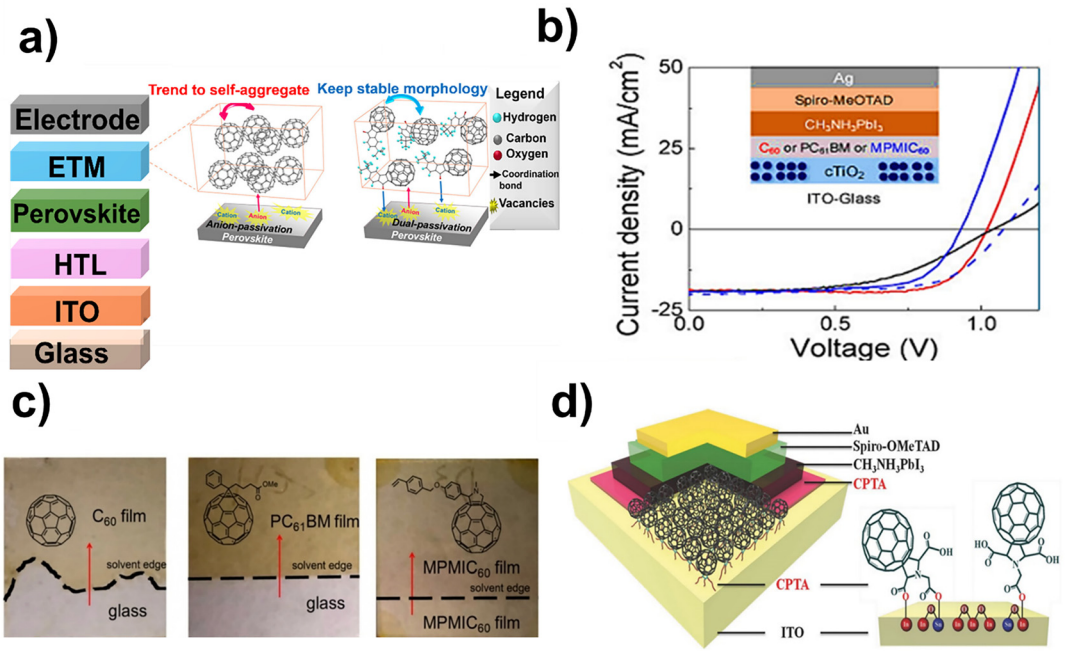

Fig. 11 (a) Performance assessment of FIDO and C_{60} in PSC applications,[147] (b) the *J*–*V* characteristics of PSCs employing cross-linked $MPMIC_{60}$, PCBM, or C60 as ETMs,[163] (c) solvent resistance analysis of cured C_{60}, PC61BM, and $MPMIC_{60}$ films,[30] and (d) a diagrammatic representation of the device architecture for planar n–i–p PSC featuring CPTA as ETM.[129]

groups (COOH and –CN) could further reduce capacitive hysteresis, yielding 13.5% PCE. Dong *et al.* showed that even simple carboxylation (PCBA) could boost TiO_2-based devices to 17.76% PCE with a remarkable 1.16 V V_{oc}, highlighting the universal effectiveness of carboxyl anchoring.[160]

The most significant advances emerged from CPTA-based systems, where carboxyl groups were leveraged for electronic and crystallographic control. Jia *et al.* established CPTA as a high-performance ETM (18.39% PCE on glass),[157] while Xu demonstrated its stability-enhancing properties on SnO_2. Wang's breakthrough CPTA : PbI_2 template system (20.20% PCE) revealed the profound impact of carboxyl coordination on perovskite nucleation, the octahedral Pb^{2+}-CPTA complexes reduced nucleation barriers,[139] producing large-grained films with exceptional uniformity (FF >80%). This epitaxial growth mechanism represents a paradigm shift in perovskite crystallization control.

4.7.2 Hydroxyl (–OH) functionalized fullerene derivatives. Hydroxyl groups have emerged as versatile polar anchors for tailoring fullerene-based interfacial layers in PSCs, complementing the more established carboxyl-functionalized analogues. Chen *et al.*'s pioneering 2016 work with fullerenol (Fig. 10a) demonstrated how multiple –OH groups could simultaneously enhance TiO_2 conductivity and perovskite wettability, establishing a template for subsequent developments.[188] The material's hydrophilic nature improved interfacial contact while its electron-rich structure facilitated charge transport, addressing two critical limitations of oxide-based ETMs.

The functionality of hydroxyl groups was further expanded through innovative molecular designs. Tong *et al.* developed a hydrophobic C9 derivative combined with a long alkyl chain with strategic –OH placement, achieving 21.3% PCE[189] in mixed-cation devices through dual action: (1) covalent bonding with undercoordinated Sn atoms passivated oxygen vacancies, while (2) the hydrophobic backbone protected the perovskite layer. This concept was refined in Wang 2023 NPC_{60}-OH, where phenolic-OH-OH-OH-OH groups optimized the SnO_2/perovskite interface, reducing the energy barrier while enlarging perovskite grains (21.39% PCE).[190] The most sophisticated implementation came from Jen's catechol-functionalized Fa, which formed Zn–O–C bridges with ZnO nanoparticles (Fig. 10c). This quasi-core–shell structure (Fa-ZnO NPs) (Fig. 11c), uniquely enhanced electron density in ZnO's conduction band through interfacial charge redistribution, demonstrating how hydroxyl chemistry can fundamentally modify oxide electronic properties (Fig. 10e).[191]

While carboxyl and hydroxyl groups share similar anchoring capabilities, hydroxyl-functionalized derivatives offer distinct advantages in moisture-sensitive applications due to their reduced acidity. The optimal spatial arrangement of these polar groups, whether in densely functionalized fullerenols or strategically placed single –OH units, remains an important area for future investigation, particularly for achieving both high efficiency (>22%) and long-term operational stability in PSCs.

4.8 Fullerene derivatives with halogen

Halogen-functionalized fullerene derivatives (Fig. 10) have emerged as vital components in enhancing the performance and stability of PSCs. The incorporation of halogen atoms into

the fullerene structure effectively tunes the electronic characteristics, particularly influencing the HOMO/LUMO energy levels.[192] This adjustment facilitates better ELA between the ETM and adjacent layers, promoting more efficient photo-induced charge transfer dynamics. Moreover, halogenation enhances the interfacial interaction and surface properties of the ETM and light-absorbing layers, which collectively contribute to improved film morphology, reinforced lattice integrity, and a reduction in interfacial defect density. These improvements are instrumental in suppressing non-radiative recombination pathways and elevating device efficiency.

Halogenated fullerene derivatives also act as effective passivation agents, mitigating both surface and interface defects that commonly lead to charge carrier recombination. Their inherent chemical robustness provides additional protection against environmental degradation, particularly from moisture and oxygen. Furthermore, these derivatives enhance charge carrier dynamics by extending carrier lifetime and improving mobility, thereby facilitating more efficient charge extraction and collection. For instance, Wang *et al.* investigated the influence of halogen substitutions, specifically hydrogen (H), chlorine (Cl), and bromine (Br), on fullerene derivatives and observed enhanced crystallinity in the perovskite layer, increased grain size, and reduced grain boundary density.[193] Notably, the incorporation of NAMF-Cl, which induces chlorination of the TiO_2 layer, promoted stronger Ti–Cl bonding and yielded a power conversion efficiency (PCE) of 19.2%. Similarly, Rajagopal *et al.* utilized a difluorinated fullerene derivative (DF-C_{60}) in the fabrication of lead–tin (Pb–Sn) binary PSCs with a narrow bandgap structure. By employing an anti-solvent method, they achieved a graded heterojunction within the perovskite film. This strategy effectively suppressed deep-state defects and improved perovskite quality, culminating in a PCE of 15.61%.[194]

4.9 Cross-linked fullerene derivatives

Fullerene derivatives are generally solubilized in organic solvents and subsequently harnessed onto the light-harvesting layer during device fabrication. However, this method can lead to the partial dissolution of both the charge collection layer and the perovskite layer, adversely affecting overall device performance. To address this issue, cross-linkable fullerene derivatives have been developed, significantly enhancing the stability of ETMs. These derivatives typically incorporate highly reactive functional groups such as styryl, vinyl, silyloxy, oxetane, thiophene, and benzocyclobutene *etc*. The cross-linking mechanisms for these groups rely on free radical or ionic reactions, triggered by stimuli such as thermal energy, UV light, or chemical initiators. Specifically, heating can induce polymerization in fullerene derivatives with styryl, vinyl, siloxyl, azide, and benzocyclobutane functionalities. Oxetane groups are known to undergo ring-opening polymerization when subjected to UV curing, creating robust cross-linked networks.

Additionally, azide groups, characterized by their highly reactive nitrogen atom, facilitate cross-linking reactions, further enhancing the structural integrity and solvent resistance of fullerene-based ETMs.

Zang *et al.* demonstrated the effectiveness of cross-linking as a modification strategy for fullerene-based ETMs. They developed a tailored fullerene derivative capable of forming an insoluble, interconnected network in aprotic solvents. This network not only preserves high electron mobility but also enhances resistance to solvent-induced dissolution, thereby significantly improving the long-term operational stability of the device.[112]

4.9.1 Thermal cross-linked (TCL) fullerene derivatives. To enhance device performance, it is essential to address the challenges encountered by other ETMs, including inadequate surface morphology (Fig. 11a), misalignment of energy levels, and insufficient adhesion to the light-harvesting layer. Xu *et al.* conducted an early investigation into a cross-linkable fullerene derivative known as 1-(*p*-phenoxy)-(*p*-methylvinylbenzene)-indolino fullerene ($MPMIC_{60}$), capable of achieving complete cross-linking upon heating to 250 °C.[121] Their findings demonstrated that cross-linked $MPMIC_{60}$ significantly improves solvent resistance and raises the fracture energy of the TiO_2 ETM compared to traditional PCBM and C_{60} films, (Fig. 11b), achieving a PCE of 13.8%. Snaith and co-workers, in 2016, incorporated two distinct cross-linked fullerene variants, namely PCBCB and sol–gel C_{60}, into PSCs. Sol–gel C_{60} underwent cross-linking *via* hydrolysis–condensation reactions, while PCBCB was cross-linked through thermal annealing at 200 °C.[195] Both processes resulted in insoluble films with improved electron-selective interfaces, reduced shunting pathways, enhanced hole-blocking properties, and optimized charge carrier dynamics, leading to a significant PCE of 17.9%.

Hong *et al.* developed another fullerene derivative, C-PCBSD (Fig. 12a), functionalized for use as a TCL, employing an anti-solvent deposition technique for integration into perovskite films. This approach improved perovskite crystallization, electron extraction efficiency, and resulted in a PCE of 17.21%.[196] Building on this approach, the authors further developed a composite film composed of C-PCBSD and graphdiyne (GD), formed *via* π–π stacking interactions. This composite exhibited enhanced electron mobility, improved energy-level alignment, and facilitated the growth of high-quality perovskite layers with increased resistance to solvent exposure. As a result, the device achieved a significantly improved PCE of 20% along with enhanced operational stability. Additionally, Kang *et al.* introduced a UV-curable cross-linked fullerene derivative, C-PCBOD, which was employed to modify the TiO_2 electron transport layer.[197] The resulting cross-linked PCBOD film (Fig. 12b) demonstrated excellent surface coverage on TiO_2 and formed a robust hydrophilic protective layer (Fig. 12c), effectively preventing solvent-induced damage during the deposition of the $CH_3NH_3PbI_3$ perovskite absorber (Fig. 12d).

Furthermore, a styrene functionalized cross-linkable fullerene derivative, $MPMIC_{60}$, was developed as an alternative to conventional ETMs like PCBM and C_{60} (Fig. 11c). Upon annealing at 250 °C, $MPMIC_{60}$ formed a solvent-resistant film with

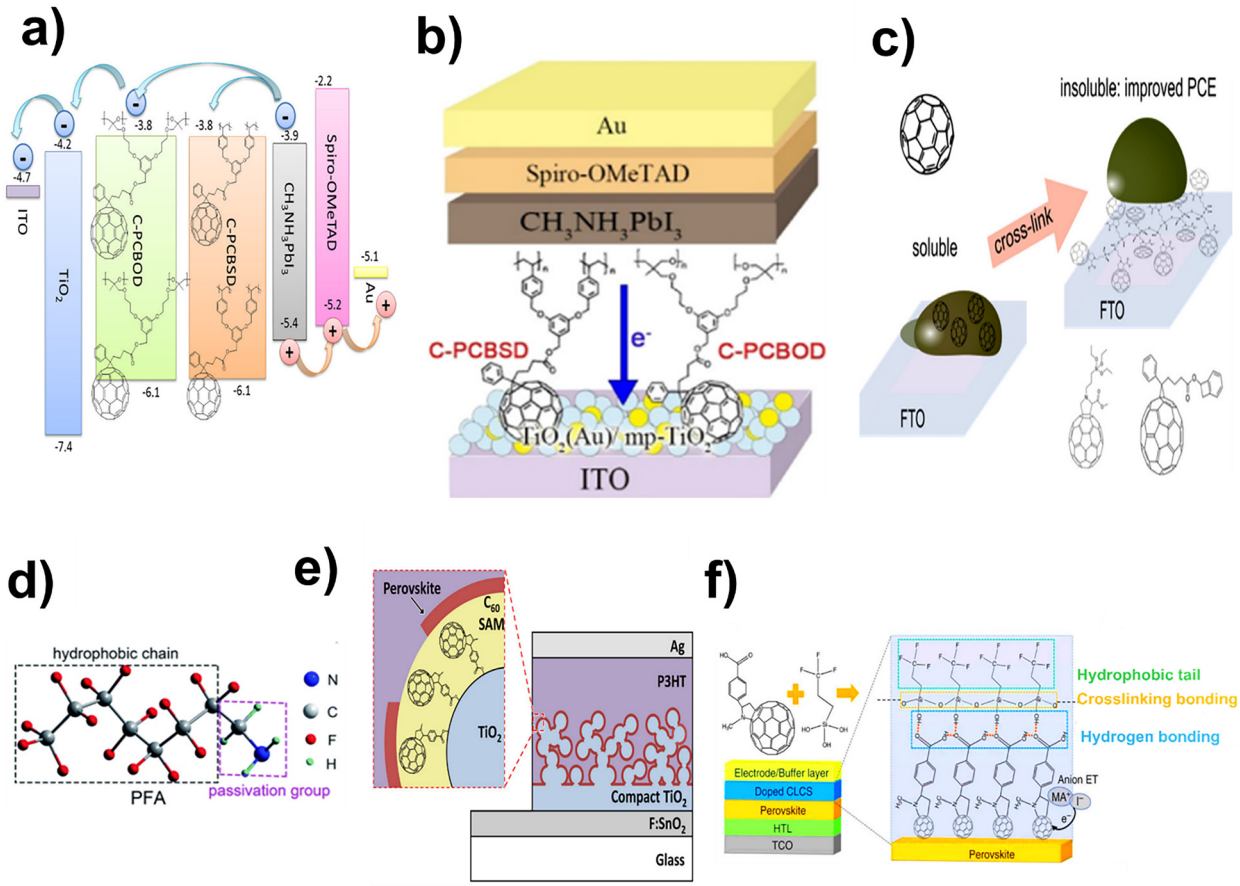

Fig. 12 (a) Schematic representation of a PSC with energy levels associated with each layer,[197] (b) passivation mechanism of C-PCBOD as an interfacial layer between TiO_2 and perovskite, (c) the molecular architectures of cross-linked and halogen functionalized fullerene,[187] (d) molecular structure of PFA,[148] diagram of the device architecture, showing C_{60}-SAM binding to the (e) TiO_2 surface and (f) its crosslinking with a silane-coupling agent.[157,187]

enhanced rupture toughness, resulting in substantial improvements in V_{oc} and J_{sc}. Giacalone *et al.* enhanced fullerene derivatives by incorporating PCL silane molecules through substituting benzoic acid groups (Fig. 12e).[198] Silane features three –OH groups in their structure. One interacts through hydrogen bonding with the –COOH group present in the C_{60} self-assembled monolayer (C_{60}-SAM), while the remaining two –OH groups partake in coupling reactions forming Si–O–Si bonds (Fig. 12f). Furthermore, introducing hydrophobic trifluoromethyl groups into silane molecules significantly enhances the water resistance of the fullerene layer.[199]

4.9.2 Photo cross-linked (PCL) fullerene derivatives. Fullerene derivatives are widely employed as organic ETMs in PSCs. However, their porous molecular structure raises concerns due to their susceptibility to moisture-induced degradation. Researchers developed TCL of functionalized fullerene with styrene moieties is widely utilized for generating active sites, while epoxy groups can undergo light-induced cross-linking.

In 2024, Cabrera-Espinoza introduced a novel functionalized fullerene designed as a cross-linkable agent for TiO_2 surface modification.[200] The UV-cured cross-linked PCBOD film notably improved surface coverage on the TiO_2 ETM, forming a moisture-resistant protective The cross-linked PCBOD interlayer effectively passivated DSs within the TiO_2, enhancing electron separation and reducing charge recombination rates, thereby achieving impressive PCEs of 18.3% and 15.9%, respectively.

Cross-linkable fullerene derivatives, specifically the [6,6]-phenyl-C61-butyric styryl dendron (PCBSD) and the [6,6]-phenyl-C61-butyric oxetane dendron (PCBOD).[201] These derivatives feature multiple cross-linking groups, allowing the formation of robust, highly cross-linked films on TiO_2 surfaces with exceptional coverage, superior solvent resistance, improved electron mobility, and effective passivation of surface defects. Devices using PCBOD-modified planar and mesoporous TiO_2 ETM achieved outstanding PCE of 15.9% and 18.3%, respectively. Cross-linking strategy utilizing 1,6-diazidohexane (DAZH) to link PCBM molecules, forming cross-linked PCBM through nitrene and C–H activation reactions.[121] This cross-linked PCBM interlayer, applied on top of the TiO_2 ETM, exhibited outstanding electron extraction properties and robust solvent resistance, thereby preventing the perovskite precursor from being displaced during spin-coating.

Consequently, PSCs with the composition (HC$(NH_2)_2)_{0.66}(CH_3NH_3)_{0.34}$-$PbI_{2.85}Br_{0.15}$ achieved PCEs of 18.4% for smaller devices and 14.9% for 4 cm^2 modules.

4.10 ICBA and ICBA-like fullerene derivatives

While PCBM remains a widely used ETM in PSCs, its limitations in ELA and interfacial recombination have spurred the exploration of alternative fullerene derivatives, notably indene-C_{60} bisadduct (ICBA) and its analogues, (Fig. 13a). These materials offer tunable lowest unoccupied molecular orbital (LUMO) levels, enhanced solubility, and improved defect passivation capabilities, addressing key challenges in PSC performance.[202] Recent studies highlight the superiority of ICBA-like derivatives over conventional PCBM. V_{oc} was optimized by introducing 4-fluoro phenethylamine hydrobromide (FPEABr) as a dipole layer, (Fig. 13b), aligning energy levels at the perovskite/ICBA interface, and achieving a PCE of 15.7%.[203]

Xing *et al.* incorporated ICBA into perovskite precursors, passivating grain boundary defects and enhancing charge extraction, achieving a PCE of 18.14% (Fig. 13c).[144] The introduction of ICBA into the perovskite grain boundaries facilitated the photocarrier dynamics of charge carriers from the perovskite layer to the ETMs, leading to an increased PCE of 18.14%. This approach allowed for a more effective alignment of the energy levels between the absorber and ICBA layers, resulting in a unilateral increase in the device's V_{oc} by one-tenth, ultimately leading to an impressive PCE record of 15.7%.[204]

T. Ji *et al.*[205] reported a modest PCE of 3.4% with ICBA, later improved to 8.06% by Liu *et al. via* bis-C_{60} doping.[131]

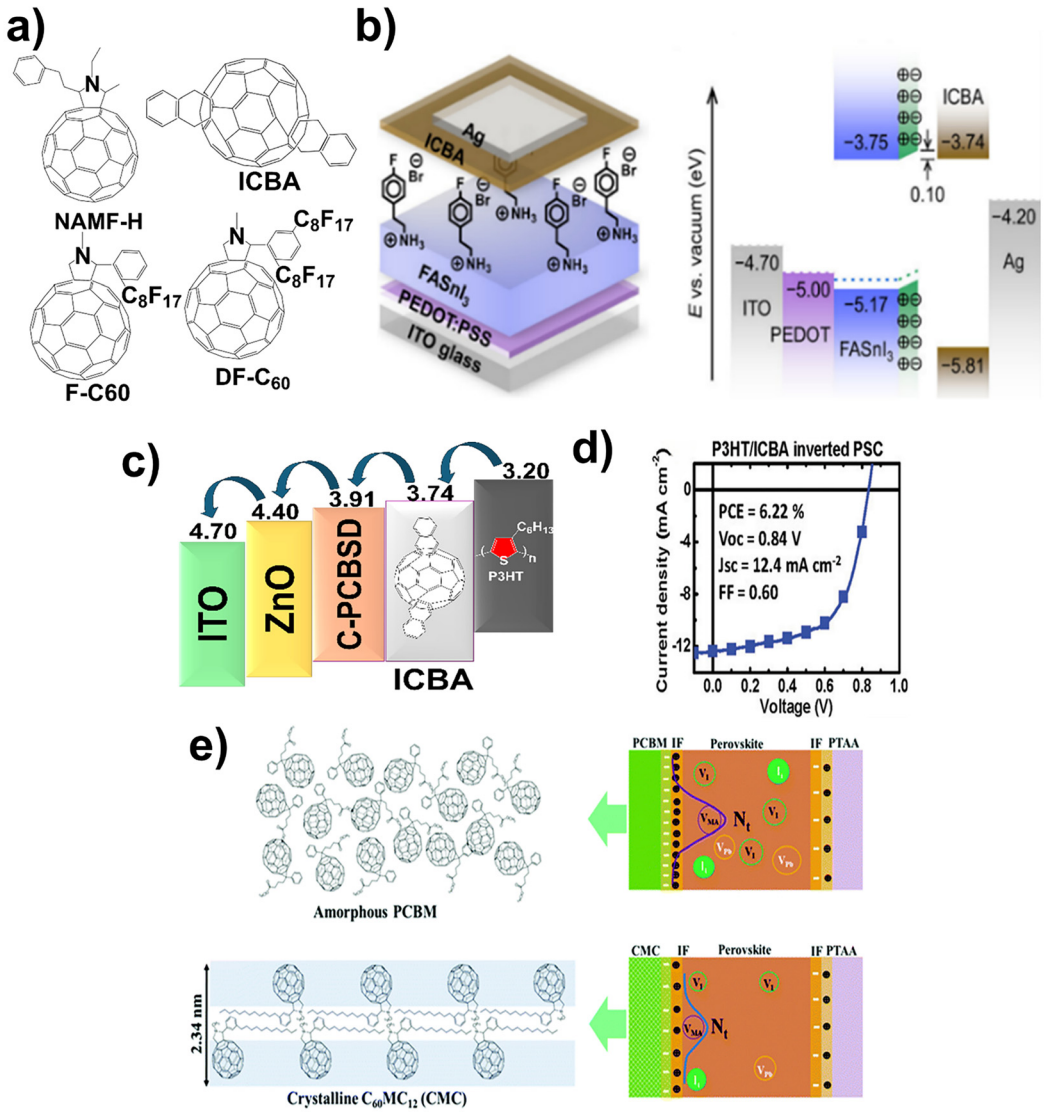

Fig. 13 (a) Molecular structure of ICBA derivatives,[204] (b) schematic depiction of the mechanism involving crystalline fullerene derivatives for enhancement in device performance,[157] (c and d) structure and energy levels of the inverted PSC, and (e) the multilayer configurations energy levels diagram, and their corresponding *J*–*V* curve.

ICBA-*trans* in wide-bandgap PSCs, achieving a PCE of 18.5% and V_{oc} of 1.21 V due to reduced energy disorder.[205] The P3HT/ICBA-based cell has demonstrated notable performance metrics, achieving a PCE of 6.22%, a V_{oc} of 0.84 V, and a J_{sc} of 12.4 mA cm^{-2} (Fig. 13d). Additionally, Ali *et al.* demonstrated that indene-C_{60}-tris adduct (ICTA) has higher LUMO level (−3.36 eV *vs.* PCBM's −3.9 eV) reduces energy loss, enhancing V_{oc}, though reduce charge extraction efficiency.[206] Marin-Beloqui *et al.* developed $C_{60}(CH_2)$(Ind), which enhanced defect passivation and electron extraction (PCE: 18.1%, V_{oc}: 1.13 V).[207]

Yang *et al.* synthesized C5-NCMA, achieving a PCE of 17.6% *via* high LUMO alignment.[208] Xie *et al.* compared derivatives EBNC (7.36%) and EDNC (12.64%), noting lower efficiencies than PCBM due to suboptimal functional groups.[209] To improve the structural stability, Li *et al.* observed that TiO_2/PCBM bilayers (PCE: 18.0%) outperform ICMA (13.9%) due to superior ELA in wide-bandgap PSCs ($E_g \approx 1.8$ eV), achieved a V_{oc} of 1.35 V and PCE of 18.9% using CMC:ICBA blends (Fig. 13e), with minimal non-radiative losses (ΔV_{oc} = 70 mV).[210] Although significant advancements have been achieved with ICBA, its effectiveness is hindered by its low electron mobility ($\sim 10^{-4}$ cm^2 V^{-1} s^{-1}) is significantly lower than PCBM's ($\sim 10^{-2}$ cm^2 V^{-1} s^{-1}), limiting charge extraction in thick films. These factors significantly impede the effective transport of charge carriers from the light-harvesting layer to the ETM.

5. Conclusions and outlook

Functionalized fullerenes have played a transformative role in advancing the efficiency and stability of PSCs, particularly through the modulation of photocarrier dynamics. Derivatives such as PCBM, and ICBA have demonstrated multifunctionality-acting not only as efficient ETMs but also as interfacial passivators that mitigate defect states and enhance charge separation. These attributes have enabled PSCs to achieve power conversion efficiencies exceeding 24%, while simultaneously improving operational stability. Spectroscopic investigations have confirmed their capability to coordinate with perovskite lattices, reduce non-radiative recombination, and facilitate robust charge transport.

Despite these achievements, several challenges remain unresolved. The impact of specific functional groups on long-range charge diffusion and electronic coupling remains poorly understood, limiting further optimization of device performance. Interfacial issues such as aggregation and energy-level mismatch continue to hinder charge extraction and promote recombination, particularly in large-area or flexible architectures. Moreover, the absence of systematic design principles for fullerene functionalization restricts the rational development of derivatives tailored to diverse PSC configurations.

In light of these limitations, non-fullerene ETMs, such as cyano-functionalized bithiophene imide dimer (CNI2)-based polymers (*e.g.*, PCNI2-BTI), offer several advantages, including excellent photothermal stability, high electron mobility, good solubility, and strong interfacial interactions with perovskite layers. These attributes have enabled the realization of PCEs exceeding 26% along with outstanding device stability, positioning non-fullerene ETMs as highly competitive alternatives to their fullerene-based counterparts. To address current limitations and drive further progress in ETM development, future research should focus on the molecular engineering of materials with tailored energy levels, enhanced passivation properties, and improved morphological compatibility. Moreover, the exploration of hybrid systems that integrate the interfacial stability of fullerene derivatives with the tunability and multifunctionality of non-fullerene materials holds significant promise. The application of advanced spectroscopic and computational techniques will also be crucial for elucidating charge transport and recombination mechanisms, thereby facilitating predictive design strategies optimized for specific device architectures.

Author contributions

Muhammad Waqas: conceptualization, visualization, writing – original draft. Dhruba B. Khadka: supervision, writing – review and editing. Abdul Haseeb Hassan Khan: literature organizing, categorizing. Ying-Chiao Wang: conceptualization, funding acquisition, supervision, writing – review and editing.

Conflicts of interest

The authors declare no competing financial interest.

Data availability

The datasets used and/or analyzed during the current study are available from the corresponding author upon reasonable request.

Acknowledgements

Y.-C. W. acknowledges the financial support from the National Science and Technology Council (NSTC), Taiwan, R.O.C. (grant no. NSTC 113-2221-E-110-005- and NSTC 112-2222-E-110-004). This work was also supported by the Taiwan Comprehensive University System (TCUS). And Y.-C. W. thanks the Yushan Fellow Program by the Ministry of Education (MOE), Taiwan for the financial support.

References

1 S. Yang, W. Fu, Z. Zhang, H. Chen and C.-Z. Li, Recent advances in perovskite solar cells: efficiency, stability and lead-free perovskite, *J. Mater. Chem. A*, 2017, 5(23), 11462–11482.

2 R. Sharif, *et al.*, A comprehensive review of the current progresses and material advances in perovskite solar cells, *Nanoscale Adv.*, 2023, **5**(15), 3803–3833.
3 C. Zuo, H. J. Bolink, H. Han, J. Huang, D. Cahen and L. Ding, Advances in perovskite solar cells, *Adv. Sci.*, 2016, **3**(7), 1500324.
4 T. Nie, Z. Fang, X. Ren, Y. Duan and S. Liu, Recent advances in wide-bandgap organic–inorganic halide perovskite solar cells and tandem application, *Nano-Micro Lett.*, 2023, **15**(1), 70.
5 F. Znidi, M. Morsy and M. N. Uddin, Navigating challenges and solutions for metal-halide and carbon-based electrodes in perovskite solar cells (NCS-MCEPSC): An environmental approach, *Heliyon*, 2024, **10**(12), e32843.
6 P. Roy, N. K. Sinha, S. Tiwari and A. Khare, A review on perovskite solar cells: Evolution of architecture, fabrication techniques, commercialization issues and status, *Sol. Energy*, 2020, **198**, 665–688.
7 D. Meng, J. Xue, Y. Zhao, E. Zhang, R. Zheng and Y. Yang, Configurable organic charge carriers toward stable perovskite photovoltaics, *Chem. Rev.*, 2022, **122**(18), 14954–14986.
8 J. Lian, B. Lu, F. Niu, P. Zeng and X. Zhan, Electron–transport materials in perovskite solar cells, *Small Methods*, 2018, **2**(10), 1800082.
9 V. S. Katta, M. Waheed and J. H. Kim, Recent advancements in enhancing interfacial charge transport for perovskite solar cells, *Sol. RRL*, 2024, **8**(7), 2300908.
10 P. W. Liang, C. C. Chueh, S. T. Williams and A. K. Y. Jen, Roles of fullerene–based interlayers in enhancing the performance of organometal perovskite thin–film solar cells, *Adv. Energy Mater.*, 2015, **5**(10), 1402321.
11 Y. Y. Lai, Y.-J. Cheng and C.-S. Hsu, Applications of functional fullerene materials in polymer solar cells, *Energy Environ. Sci.*, 2014, **7**(6), 1866–1883.
12 X.-J. Kong, L.-S. Long, Z. Zheng, R.-B. Huang and L.-S. Zheng, Keeping the ball rolling: fullerene-like molecular clusters, *Acc. Chem. Res.*, 2010, **43**(2), 201–209.
13 P. Schwerdtfeger, L. N. Wirz and J. Avery, The topology of fullerenes, *Wiley Interdiscip. Rev.: Comput. Mol. Sci.*, 2015, **5**(1), 96–145.
14 Y. R. Yao, O. Fernandez-Delgado and L. Echegoyen, Fullerenes and their applications, in *Handbook of Carbon-Based Nanomaterials*, Elsevier, 2021, vol. 1, pp. 19–158.
15 Z. C. Chen, Y.-Z. Tan and S.-Y. Xie, Fullerenes violating the isolated pentagon rule, in *Handbook of Fullerene Science and Technology*, Springer, 2022, vol. 1, pp. 181–217.
16 J. Zhao, Q. Du, S. Zhou and V. Kumar, Endohedrally doped cage clusters, *Chem. Rev.*, 2020, **120**(17), 9021–9163.
17 Y. Z. Tan, *et al.*, Chlorofullerenes featuring triple sequentially fused pentagons, *Nat. Chem.*, 2010, **2**(4), 269–273.
18 Y. Zhang, *et al.*, Structural, electronic, and nonlinear optical properties of $C_{66}H_4$ and C70Cl6 encapsulating Li and F atoms, *ACS Omega*, 2021, **6**(24), 16234–16240.
19 F. N. de Sousa, D. E. A. Rodrigues, F. M. de Vasconcelos, V. Meunier and E. C. Girão, Electronic properties of carbon nanostructures based on bipartite nanocage units, *Chem. Phys.*, 2024, **580**, 112206.
20 A. Mahmoodpoor, *et al.*, Ionic liquid gating in perovskite solar cells with fullerene/carbon nanotube collectors, *Energy Technol.*, 2022, **10**(9), 2200485.
21 L. Feng, K.-Y. Wang, G. S. Day and H.-C. Zhou, The chemistry of multi-component and hierarchical framework compounds, *Chem. Soc. Rev.*, 2019, **48**(18), 4823–4853.
22 R. Zahran and Z. Hawash, Fullerene–based inverted perovskite solar cell: a key to achieve promising, stable, and efficient photovoltaics, *Adv. Mater. Interfaces*, 2022, **9**(35), 2201438.
23 Y. Fang, C. Bi, D. Wang and J. Huang, The functions of fullerenes in hybrid perovskite solar cells, *ACS Energy Lett.*, 2017, **2**(4), 782–794.
24 L. Fu, H. Li, L. Wang, R. Yin, B. Li and L. Yin, Defect passivation strategies in perovskites for an enhanced photovoltaic performance, *Energy Environ. Sci.*, 2020, **13**(11), 4017–4056.
25 Y. Zhong, *et al.*, Inhibition of ion migration for highly efficient and stable perovskite solar cells, *Adv. Mater.*, 2023, **35**(52), 2302552.
26 Y. Zhao, W. Zhou, Z. Han, D. Yu and Q. Zhao, Effects of ion migration and improvement strategies for the operational stability of perovskite solar cells, *Phys. Chem. Chem. Phys.*, 2021, **23**(1), 94–106.
27 J. Thiesbrummel, *et al.*, Ion-induced field screening as a dominant factor in perovskite solar cell operational stability, *Nat. Energy*, 2024, **9**(6), 664–676.
28 W. Zhang, *et al.*, Modular functionalization of carbon nanotubes and fullerenes, *J. Am. Chem. Soc.*, 2009, **131**(24), 8446–8454.
29 D. Pantarotto, N. Tagmatarchis, A. Bianco and M. Prato, Synthesis and biological properties of fullerene-containing amino acids and peptides, *Mini-Rev. Med. Chem.*, 2004, **4**(7), 805–814.
30 G. Zhou, *et al.*, Recent Progress on Cross–Linkable Fullerene–Based Electron Transport Materials for Perovskite Solar Cells, *ChemSusChem*, 2025, **18**(3), e202401629.
31 H. Wang, C. Zhang, Y. Yao, C. Cheng and K. Wang, Non–Fullerene Organic Electron Transport Materials toward Stable and Efficient Inverted Perovskite Photovoltaics, *Small*, 2024, **20**(43), 2403193.
32 H. Si, X. Zhao, Z. Zhang, Q. Liao and Y. Zhang, Low-temperature electron-transporting materials for perovskite solar cells: fundamentals, progress, and outlook, *Coord. Chem. Rev.*, 2024, **500**, 215502.
33 H. Wang, Z. Zhang, C. Zhang, Y. Yao and K. Wang, Structural modification of fullerene derivates for high-performance inverted perovskite solar cells, *J. Mater. Chem. A*, 2024, **12**, 22442–22457.
34 Y. Li, *et al.*, A review on morphology engineering for highly efficient and stable hybrid perovskite solar cells, *J. Mater. Chem. A*, 2018, **6**(27), 12842–12875.

35 B. Chen, S. Wang, Y. Song, C. Li and F. Hao, A critical review on the moisture stability of halide perovskite films and solar cells, *Chem. Eng. J.*, 2022, **430**, 132701.
36 L. Zang, C. Zhao, X. Hu, J. Tao, S. Chen and J. Chu, Emerging trends in electron transport layer development for stable and efficient perovskite solar cells, *Small*, 2024, **20**(26), 2400807.
37 Y. C. Wang, *et al.*, Quantum-assisted photoelectric gain effects in perovskite solar cells, *NPG Asia Mater.*, 2020, **12**(1), 54.
38 Z. Xiao, *et al.*, Thin-film semiconductor perspective of organometal trihalide perovskite materials for high-efficiency solar cells, *Mater. Sci. Eng., R*, 2016, **101**, 1–38.
39 H. Lu, *et al.*, High-Quality PEI/Ag/PEI-Zn Semitransparent Electrode for Efficient ITO-Free Flexible Organic Solar Cells and Perovskite Solar Cells, *IEEE J. Photovoltaics*, 2024, **15**(1), 46–53.
40 L. V. T. Merino, *et al.*, Impact of the valence band energy alignment at the hole-collecting interface on the photostability of wide band-gap perovskite solar cells, *Joule*, 2024, **8**(9), 2585–2606.
41 T. Wang, W. Deng, J. Cao and F. Yan, Recent progress on heterojunction engineering in perovskite solar cells, *Adv. Energy Mater.*, 2023, **13**(33), 2201436.
42 P. Murugan, T. Hu, X. Hu and Y. Chen, Advancements in organic small molecule hole-transporting materials for perovskite solar cells: past and future, *J. Mater. Chem. A*, 2022, **10**(10), 5044–5081.
43 V. Manjunath, S. Bimli, P. A. Shaikh, S. B. Ogale and R. S. Devan, Understanding the role of inorganic carrier transport layer materials and interfaces in emerging perovskite solar cells, *J. Mater. Chem. C*, 2022, **10**(42), 15725–15780.
44 S. Kumar, *et al.*, Recent advances in perovskite materials: exploring multifaceted properties for energy harvesting applications, *Ionics*, 2024, **30**(9), 5159–5188.
45 S. Kumar, *et al.*, Recent advances in perovskite materials: exploring multifaceted properties for energy harvesting applications, *Ionics*, 2024, **30**, 1–30.
46 A. K. Jena, A. Kulkarni and T. Miyasaka, Halide perovskite photovoltaics: background, status, and future prospects, *Chem. Rev.*, 2019, **119**(5), 3036–3103.
47 C. Dormann, M. F. Dollard and M. A. Idris, PSC; current status and implications for future research, in *Psychosocial Safety Climate: A new work stress theory*, 2019, vol. 1, pp. 431–449.
48 M. I. Omer, *et al.*, Two quasi-interfacial pn junctions observed by a dual-irradiation system in perovskite solar cells, *npj Flexible Electron.*, 2023, **7**(1), 23.
49 D. Ramirez, *et al.*, Meso-superstructured perovskite solar cells: revealing the role of the mesoporous layer, *J. Phys. Chem. C*, 2018, **122**(37), 21239–21247.
50 C. Zhang, *et al.*, Exploring the Potential and Hurdles of Perovskite Solar Cells with pin Structure, *ACS Nano*, 2024, **18**(47), 32299–32314.
51 A. K. Al-Mousoi and M. K. Mohammed, Engineered surface properties of MAPI using different antisolvents for hole transport layer-free perovskite solar cell (HTL-free PSC), *J. Sol-Gel Sci. Technol.*, 2020, **96**, 659–668.
52 S. Jiang, *et al.*, Interfacial Energetics Reversal Strategy for Efficient Perovskite Solar Cells, *Adv. Mater.*, 2025, **1**, 2503110.
53 S. Aftab, H. H. Hegazy, M. Z. Iqbal, M. W. Iqbal, G. Nazir and S. Hussain, Recent advances in dynamic homojunction PIN diodes based on 2D materials, *Adv. Mater. Interfaces*, 2023, **10**(6), 2201937.
54 S. Bhattarai, *et al.*, A detailed review of perovskite solar cells: Introduction, working principle, modelling, fabrication techniques, future challenges, *Micro Nanostruct.*, 2022, **172**, 207450.
55 H. Wang, *et al.*, Reducing the Depletion Region Width at the Anode Interface via a Highly Doped Conjugated Polyelectrolyte Composite for Efficient Organic Solar Cells, *ACS Appl. Mater. Interfaces*, 2024, **16**(3), 3744–3754.
56 G. A. Sibu, P. Gayathri, T. Akila, R. Marnadu and V. Balasubramani, Manifestation on the choice of a suitable combination of MIS for proficient Schottky diodes for optoelectronics applications: A comprehensive review, *Nano Energy*, 2024, **125**, 109534.
57 M. Abbas, X. Xu, M. Rauf and A. K. K. Kyaw, A Comprehensive Review on Defects-Induced Voltage Losses and Strategies toward Highly Efficient and Stable Perovskite Solar Cells, in *Photonics*, 2024, vol. 11, ((no. 1)), p. 87.
58 P. Kumar, V. K. Shukla, M. Kim and R. Singh, A comprehensive review on dark current in perovskite photodetectors: Origin, drawbacks, and reducing strategies, *Sens. Actuators, A*, 2024, **369**, 115076.
59 Y. Wang, Q. Song, D. Li, Y. Liu, Y. Wang and Y. Chen, Strategies for Suppressing Dark Current of Perovskite Photodiodes towards Reliable Optoelectronic Applications, *J. Mater. Chem. C*, 2024, **12**, 10775–10805.
60 A. Morteza Najarian, M. Vafaie, B. Chen, F. P. García de Arquer and E. H. Sargent, Photophysical properties of materials for high-speed photodetection, *Nat. Rev. Phys.*, 2024, **6**(4), 219–230.
61 V. S. Menon and A. Krishnamoorthy, Hole Selectivity of n–Type Molybdenum Oxide Carrier Selective Layer for Commercial and Emerging Thin–Film Photovoltaics: A Critical Analysis of Interface Energetics and Ensuant Device Physics, *Energy Technol.*, 2023, **11**(11), 2300608.
62 H. Zhang and N.-G. Park, Progress and issues in pin type perovskite solar cells, *DeCarbon*, 2023, **3**, 100025.
63 K. Anoop and T. Ahipa, Recent advancements in the hole transporting layers of perovskite solar cells, *Sol. Energy*, 2023, **263**, 111937.
64 J. Suo, B. Yang and A. Hagfeldt, Passivation strategies through surface reconstruction toward highly efficient and stable perovskite solar cells on nip architecture, *Energies*, 2021, **14**(16), 4836.
65 J. Zhou, *et al.*, Highly efficient and stable perovskite solar cells via a multifunctional hole transporting material, *Joule*, 2024, **8**(6), 1691–1706.

66 Z. Chen, *et al.*, Perovskite grain–boundary manipulation using room–temperature dynamic self–healing "ligaments" for developing highly stable flexible perovskite solar cells with 23.8% efficiency, *Adv. Mater.*, 2023, **35**(18), 2300513.
67 J. Park, *et al.*, Controlled growth of perovskite layers with volatile alkylammonium chlorides, *Nature*, 2023, **616**(7958), 724–730.
68 C. Zhao, *et al.*, Stabilization of highly efficient perovskite solar cells with a tailored supramolecular interface, *Nat. Commun.*, 2024, **15**(1), 7139.
69 X. Liu, T. Wu, C. Zhang, Y. Zhang, H. Segawa and L. Han, Interface energy–level management toward efficient tin perovskite solar cells with hole–transport–layer–free structure, *Adv. Funct. Mater.*, 2021, **31**(50), 2106560.
70 T. A. Chowdhury, M. A. B. Zafar, M. S.-U. Islam, M. Shahinuzzaman, M. A. Islam and M. U. Khandaker, Stability of perovskite solar cells: issues and prospects, *RSC Adv.*, 2023, **13**(3), 1787–1810.
71 G. D. Tabi, *et al.*, Fluorinated polymer additives in Spiro-OMeTAD to improve the efficiency and stability of perovskite solar cells, *Chem. Eng. J.*, 2024, **482**, 149062.
72 D. B. Khadka, *et al.*, Coordination Nanosheets Stabilizing Efficient Tin-Based Perovskite Solar Cells, *ACS Appl. Mater. Interfaces*, 2025, **17**(18), 26813–26822.
73 G. G. Njema, J. K. Kibet and S. M. Ngari, A review of interface engineering characteristics for high performance perovskite solar cells, *Meas.: Energy*, 2024, **2**, 100005.
74 Y. Zhang, *et al.*, Gelation of hole transport layer to improve the stability of perovskite solar cells, *Nano-Micro Lett.*, 2023, **15**(1), 175.
75 V. S. Menon, S. Ganesan, R. K. Raman, A. Alagumalai and A. Krishnamoorthy, Halogen doping of p-type inorganic hole transport layer: electronic nature-based dopant engineering for modulating hole selectivity in inverted planar perovskite solar cells, *J. Mater. Chem. C*, 2024, **12**(20), 7306–7324.
76 S. Akel, A. Kulkarni, U. Rau and T. Kirchartz, Relevance of long diffusion lengths for efficient halide perovskite solar cells, *PRX Energy*, 2023, **2**(1), 013004.
77 S. P. Senanayak, *et al.*, Charge transport in mixed metal halide perovskite semiconductors, *Nat. Mater.*, 2023, **22**(2), 216–224.
78 J. Kim, A. J. Yun, B. Park and J. Kim, Recent progress in carbon electrodes for efficient and cost-benign perovskite optoelectronics, *Electron. Mater. Lett.*, 2022, **18**(3), 232–255.
79 J. Liu, T. Ye, D. Yu, S. Liu and D. Yang, Recoverable Flexible Perovskite Solar Cells for Next–Generation Portable Power Sources, *Angew. Chem.*, 2023, **135**(40), e202307225.
80 S. S. Kahandal, *et al.*, Perovskite Solar Cells: Fundamental Aspects, Stability Challenges, and Future Prospects, *Prog. Solid State Chem.*, 2024, **74**, 100463.
81 X. Yu, *et al.*, Numerical simulation analysis of effect of energy band alignment and functional layer thickness on the performance for perovskite solar cells with $Cd_{1-x}Zn_xS$ electron transport layer, *Mater. Res. Express*, 2020, **7**(10), 105906.
82 Y. Huang, *et al.*, Towards simplifying the device structure of high–performance perovskite solar cells, *Adv. Funct. Mater.*, 2020, **30**(28), 2000863.
83 N. G. Park, Towards Stable, 30% Efficient Perovskite Solar Cells, *Korean J. Chem. Eng.*, 2024, **41**, 1–12.
84 C. Zhang, *et al.*, Work function tuning of a weak adhesion homojunction for stable perovskite solar cells, *Joule*, 2024, **8**(5), 1394–1411.
85 B. Wang, *et al.*, The charge carrier dynamics, efficiency and stability of two-dimensional material-based perovskite solar cells, *Chem. Soc. Rev.*, 2019, **48**(18), 4854–4891.
86 J. Xia, M. Sohail and M. K. Nazeeruddin, Efficient and stable perovskite solar cells by tailoring of interfaces, *Adv. Mater.*, 2023, **35**(31), 2211324.
87 H. Zhang and N.-G. Park, Progress and issues in pin type perovskite solar cells, *DeCarbon*, 2024, **3**, 100025.
88 Y. Pu, H. Su, C. Liu, M. Guo, L. Liu and H. Fu, A review on buried interface of perovskite solar cells, *Energies*, 2023, **16**(13), 5015.
89 G. J. Aalbers, T. P. van der Pol, K. Datta, W. H. Remmerswaal, M. M. Wienk and R. A. Janssen, Effect of sub-bandgap defects on radiative and non-radiative open-circuit voltage losses in perovskite solar cells, *Nat. Commun.*, 2024, **15**(1), 1276.
90 R. Hidayat, *et al.*, Revealing the charge carrier kinetics in perovskite solar cells affected by mesoscopic structures and defect states from simple transient photovoltage measurements, *Sci. Rep.*, 2020, **10**(1), 19197.
91 H. Wang, *et al.*, Photomechanically accelerated degradation of perovskite solar cells, *Energy Environ. Sci.*, 2025, **18**(5), 2254–2263.
92 L. Hu, *et al.*, Doping of ZnO Electron Transport Layer with Organic Dye Molecules to Enhance Efficiency and Photo–Stability of the Non–Fullerene Organic Solar Cells, *Small*, 2024, **20**(21), 2310125.
93 Y. Yu, J. Xia and Y. Liang, Basic understanding of perovskite solar cells and passivation mechanism, *AIP Adv.*, 2022, **12**(5), 055307.
94 P. Zhao, B. J. Kim and H. S. Jung, Passivation in perovskite solar cells: A review, *Mater. Today Energy*, 2018, **7**, 267–286.
95 L. Wan, *et al.*, Efficient light harvesting with a nanostructured organic electron-transporting layer in perovskite solar cells, *Nanoscale*, 2019, **11**(19), 9281–9286.
96 F. Rehman, *et al.*, Fourth-generation solar cells: a review, *Energy Adv.*, 2023, **2**(9), 1239–1262.
97 N. K. Singh and A. Agarwal, Performance assessment of sustainable highly efficient $CsSn_{0.5}Ge_{0.5}I_3/FASnI_3$ based Perovskite Solar Cell: A numerical modelling approach, *Opt. Mater.*, 2023, **139**, 113822.
98 F. Pakravesh and M. Izadyar, Molecular engineering of inorganic halide perovskites and HTMs for photovoltaic applications, *Int. J. Quantum Chem.*, 2024, **124**(1), e27239.

99 E. F. Sawires, *et al.*, Exploring various Integration Methods of carbon quantum dots in CsPbCl3 perovskite solar cells for enhanced power conversion efficiency, *J. Mater. Sci.: Mater. Electron.*, 2024, **35**(11), 1–16.
100 S. S. Birajdar, K. Bhardwaj, R. Kumar, M. Al Kobaisi, S. V. Bhosale and S. V. Bhosale, An efficient electron transport properties of fullerene functionalized with tricyanovinyldihydrofuran (TCF), *Mater. Res. Bull.*, 2022, **147**, 111644.
101 A. H. H. Khan and Y. C. Wang, Tailoring transporters for all-inorganic tin-based perovskite solar cells with efficiency exceeding 22% using SCAPS-1D simulator, *Inorg. Chem. Commun.*, 2025, **179**, 114707.
102 H. Khan and M. U. H. Shah, Modification strategies of TiO_2 based photocatalysts for enhanced visible light activity and energy storage ability, A Review, *J. Environ. Chem. Eng.*, 2023, **11**, 111532.
103 Y. Sari, P. L. Gareso, B. Armynah and D. Tahir, A review of TiO_2 photocatalyst for organic degradation and sustainable hydrogen energy production, *Int. J. Hydrogen Energy*, 2023, **55**, 984–996.
104 A. K. Chakraborty, S. Ganguli and M. A. Sabur, Nitrogen doped titanium dioxide (N-TiO_2): Electronic band structure, visible light harvesting and photocatalytic applications, *J. Water Process Eng.*, 2023, **55**, 104183.
105 S. Gouthaman and K. J. Thomas, Metal Oxide Nanostructures as an Electron Transport Layer for Dye-Sensitized Solar Cells, in *Optical Properties of Metal Oxide Nanostructures*, Springer, 2023, vol. 1, pp. 223–262.
106 F. V. Maziviero, *et al.*, Advancements and Prospects in Perovskite Solar Cells: From Hybrid to All-Inorganic Materials, *Nanomaterials*, 2024, **14**(4), 332.
107 K. Kato, N. Nagatsuka and K. Fukutani, H_2 Molecule Generation from Dissociatively Adsorbed Water on TiO_2 through Photoexcitation, *J. Phys. Chem. C*, 2024, **128**(20), 8188–8198.
108 N. A. Z. Abidin, *et al.*, Dopant engineering for ZnO electron transport layer towards efficient perovskite solar cells, *RSC Adv.*, 2023, **13**(48), 33797–33819.
109 C. Qiu, Y. Wu, J. Song, W. Wang and Z. Li, Efficient planar perovskite solar cells with ZnO electron transport layer, *Coatings*, 2022, **12**(12), 1981.
110 L. Derbali, F. Bouhjar, A. Derbali and B. Soucase, Enhanced ZnO-based ETL and nanostructured interface modification for improved perovskite solar cells efficiency, *Opt. Mater.*, 2023, **145**, 114440.
111 F. Behrouznejad, *et al.*, Modification of copper-based chalcogenide nanocrystals' interconnections for efficient hole transportation in Perovskite solar cell, *Mater. Res. Bull.*, 2024, **178**, 112892.
112 L. Zang, C. Zhao, X. Hu, J. Tao, S. Chen and J. Chu, Emerging Trends in Electron Transport Layer Development for Stable and Efficient Perovskite Solar Cells, *Small*, 2024, **20**(26), 2400807.
113 A. Ghosh, *et al.*, Improving the power conversion efficiency of $RbPbBr_3$ absorber based solar cells through the variation of efficient hole transport layers, *J. Phys. Chem. Solids*, 2024, **193**, 112179.
114 D. Stock, N. Weinberger, F. Ruske, L. Haug, M. Harnisch and R. Lackner, Development of direct current magnetron sputtered TiO_{2-x} thin films as buffer layers for copper indium gallium diselenide based solar cells, *Thin Solid Films*, 2023, **786**, 140115.
115 B. K. Mohammed, M. K. Mohammed and D. S. Ahmed, Efficient planar mixed-cation perovskite photovoltaics with low-temperature-processed indium sulfide as electron transport material, *Solid-State Electron.*, 2023, **204**, 108640.
116 S. Ijaz, *et al.*, Numerical simulation to optimize the efficiency of HTM-free perovskite solar cells by ETM engineering, *Sol. Energy*, 2023, **250**, 108–118.
117 V. P. Hoang Huy, T. M. H. Nguyen and C. W. Bark, Recent Advances of Doped SnO_2 as Electron Transport Layer for High-Performance Perovskite Solar Cells, *Materials*, 2023, **16**(18), 6170.
118 B. Yang, S. Peng and W. C. Choy, Inorganic top electron transport layer for high performance inverted perovskite solar cells, *EcoMat*, 2021, **3**(5), e12127.
119 V. P. Hoang Huy and C. W. Bark, Review on surface modification of SnO_2 electron transport layer for high-efficiency perovskite solar cells, *Appl. Sci.*, 2023, **13**(19), 10715.
120 Y. Wang, J. Wan, J. Ding, J. S. Hu and D. Wang, A rutile TiO_2 electron transport layer for the enhancement of charge collection for efficient perovskite solar cells, *Angew. Chem., Int. Ed.*, 2019, **58**(28), 9414–9418.
121 B. Xu, *et al.*, Recent Progress on Cross–Linkable Fullerene–based Electron Transport Materials for Perovskite Solar Cells, *ChemSusChem*, 2025, **18**(3), e202401629.
122 S. Zhang, *et al.*, Barrier designs in perovskite solar cells for long–term stability, *Adv. Energy Mater.*, 2020, **10**(35), 2001610.
123 J. Wei, *et al.*, Mechanisms and suppression of photo-induced degradation in perovskite solar cells, *Adv. Energy Mater.*, 2021, **11**(3), 2002326.
124 S. M. Hassan, A. I. Ahmed and M. A. Mannaa, Structural, photocatalytic, biological and catalytic properties of SnO_2/TiO_2 nanoparticles, *Ceram. Int.*, 2018, **44**(6), 6201–6211.
125 S. U. Rehman, S. Musuvadhi Babulal, D. Dabur and H.-F. Wu, Hierarchically Designed Polydopamine@Co_3O_4–SnO_2-Anchored Cellulose Photothermal Sponge for Efficient Interfacial Solar Steam Generation, *ACS ES&T Water*, 2023, **4**(1), 134–145.
126 M. Muzakir, *et al.*, Inorganic solid electrolytes for all-solid-state sodium/lithium-ion batteries: recent development and applications, *J. Mater. Chem. A*, 2024, **13**(1), 5.
127 G. K. Dalapati, *et al.*, Tin oxide for optoelectronic, photovoltaic and energy storage devices: a review, *J. Mater. Chem. A*, 2021, **9**(31), 16621–16684.
128 P. C. Huang, *et al.*, Visualizing band alignment across 2D/3D perovskite heterointerfaces of solar cells with light-

modulated scanning tunneling microscopy, *Nano Energy*, 2021, **89**, 106362.
129 Y. C. Wang, X. Li, L. Zhu, X. Liu, W. Zhang and J. Fang, Efficient and hysteresis–free perovskite solar cells based on a solution processable polar fullerene electron transport layer, *Adv. Energy Mater.*, 2017, **7**(21), 1701144.
130 Y. Gao, *et al.*, Flexible perovskite solar cells: From materials and device architectures to applications, *ACS Energy Lett.*, 2022, **7**(4), 1412–1445.
131 J. Liu, L. Qiu and S. Shao, Emerging electronic applications of fullerene derivatives: an era beyond OPV, *J. Mater. Chem. C*, 2021, **9**(45), 16143–16163.
132 H. Wang, C. Zhang, Y. Yao, C. Cheng and K. Wang, Non–Fullerene Organic Electron Transport Materials toward Stable and Efficient Inverted Perovskite Photovoltaics, *Small*, 2024, **20**(43), 2403193.
133 A. Islam, K. Usman, Z. Haider, M. F. Alam, A. Nawaz and P. Sonar, Biomass–Derived Materials for Interface Engineering in Organic/Perovskite Photovoltaic and Light–Emitting Devices, *Adv. Mater. Technol.*, 2023, **8**(7), 2201390.
134 S. Ge, *et al.*, A review on the progress of optoelectronic devices based on TiO_2 thin films and nanomaterials, *Nanomaterials*, 2023, **13**(7), 1141.
135 S. You, *et al.*, C_{60}-based ionic salt electron shuttle for high-performance inverted perovskite solar modules, *Science*, 2025, eadv4701.
136 A. V. Baskar, *et al.*, Self–assembled fullerene nanostructures: synthesis and applications, *Adv. Funct. Mater.*, 2022, **32**(6), 2106924.
137 K. Feng, *et al.*, Non-fullerene electron-transporting materials for high-performance and stable perovskite solar cells, *Nat. Mater.*, 2025, **24**, 770–777.
138 M. Ai, M. Chen and S. Yang, Recent Advances in Functionalized Fullerenes in Perovskite Solar Cells, *Chin. J. Chem.*, 2023, **41**(18), 2337–2353.
139 Y. C. Wang, J. Chang, L. Zhu, X. Li, C. Song and J. Fang, Electron–transport–layer–assisted crystallization of perovskite films for high–efficiency planar heterojunction solar cells, *Adv. Funct. Mater.*, 2018, **28**(9), 1706317.
140 C. Lee, Y. Seo, J. Han, J. Hwang and I. Jeon, Perspectives on critical properties of fullerene derivatives for rechargeable battery applications, *Carbon*, 2023, **210**, 118041.
141 X. Yin, Z. Wang, Y. Zhao, S. Zhang, Y. Zhang and Y. Song, Cross-linking polymerization boosts the performance of perovskite solar cells: from material design to performance regulation, *Energy Environ. Sci.*, 2023, **16**(10), 4251–4279.
142 T. Cao, *et al.*, Interfacial engineering via inserting functionalized water-soluble fullerene derivative interlayers for enhancing the performance of perovskite solar cells, *J. Mater. Chem. A*, 2018, **6**(8), 3435–3443.
143 J. Chang, Y.-C. Wang, C. Song, L. Zhu, Q. Guo and J. Fang, Carboxylic ester-terminated fulleropyrrolidine as an efficient electron transport material for inverted perovskite solar cells, *J. Mater. Chem. C*, 2018, **6**(26), 6982–6987.
144 Z. Xing, S.-H. Li and S. Yang, Targeted molecular design of functionalized fullerenes for high–performance and stable perovskite solar cells, *Small Struct.*, 2022, **3**(6), 2200012.
145 Z. Saki, *et al.*, The synergistic effect of dimethyl sulfoxide vapor treatment and C_{60} electron transporting layer towards enhancing current collection in mixed-ion inverted perovskite solar cells, *J. Power Sources*, 2018, **405**, 70–79.
146 Abd. Rashid bin Mohd Yusoff, M. Vasilopoulou, D. G. Georgiadou, L. C. Palilis, A. Abate and M. K. Nazeeruddin, Passivation and process engineering approaches of halide perovskite films for high efficiency and stability perovskite solar cells, *Energy Environ. Sci.*, 2021, **14**(5), 2906–2953.
147 Q.-J. Shui, *et al.*, Evaporable fullerene indanones with controlled amorphous morphology as electron transport layers for inverted perovskite solar cells, *J. Am. Chem. Soc.*, 2023, **145**(50), 27307–27315.
148 P. Guo, *et al.*, Surface & grain boundary co-passivation by fluorocarbon based bifunctional molecules for perovskite solar cells with efficiency over 21%, *J. Mater. Chem. A*, 2019, **7**(6), 2497–2506.
149 C. Tian, *et al.*, Fullerene derivative with a branched alkyl chain exhibits enhanced charge extraction and stability in inverted planar perovskite solar cells, *New J. Chem.*, 2018, **42**(4), 2896–2902.
150 C. Tian, *et al.*, Fullerene derivative with flexible alkyl chain for efficient tin-based perovskite solar cells, *Nanomaterials*, 2022, **12**(3), 532.
151 A. D. Khan, *et al.*, Advancements in the stability, protection and lead-free strategies of perovskite solar cells: a critical review, *Environ. Sci. Adv.*, 2024, **3**(7), 1004–1029.
152 W. Zhang, *et al.*, Strategies for improving efficiency and stability of inverted perovskite solar cells, *Adv. Mater.*, 2024, **36**(37), 2311025.
153 H.-J. Yu, *et al.*, Light-soaking effects and capacitance profiling in Cu (In, Ga) Se_2 thin-film solar cells with chemical-bath-deposited ZnS buffer layers, *Phys. Chem. Chem. Phys.*, 2016, **18**(48), 33211–33217.
154 A. Soultati, *et al.*, Interfacial engineering for organic and perovskite solar cells using molecular materials, *J. Phys. D: Appl. Phys.*, 2020, **53**(26), 263001.
155 S.-K. Huang, *et al.*, Unravelling the origin of the photocarrier dynamics of fullerene-derivative passivation of SnO_2 electron transporters in perovskite solar cells, *J. Mater. Chem. A*, 2020, **8**(44), 23607–23616.
156 M. Bouachrine, N. Belghiti, M. Nassiri Bennani, S. Bouzzine and M. Hamidi, The DFT chemical investigations of optoelectronic and photovoltaic properties of short-chain conjugated molecules, *Phys. Chem. Res.*, 2014, **2**(1), 11–20.
157 L. Jia, M. Chen and S. Yang, Functionalization of fullerene materials toward applications in perovskite solar cells, *Mater. Chem. Front.*, 2020, **4**(8), 2256–2282.

158 O. Fernandez-Delgado, *et al.*, Variation of interfacial interactions in PCBM-like electron-transporting compounds for perovskite solar cells, *ACS Appl. Mater. Interfaces*, 2019, **11**(37), 34408–34415.
159 K. Wojciechowski, *et al.*, Cross-linkable fullerene derivatives for solution-processed n–i–p perovskite solar cells, *ACS Energy Lett.*, 2016, **1**(4), 648–653.
160 Y. Dong, *et al.*, Highly efficient planar perovskite solar cells via interfacial modification with fullerene derivatives, *Small*, 2016, **12**(8), 1098–1104.
161 X. Liu, M. Lei, Y. Zhou, B. Song and Y. Li, High performance planar pin perovskite solar cells with crown-ether functionalized fullerene and LiF as double cathode buffer layers, *Appl. Phys. Lett.*, 2015, **107**(6), 063901.
162 S. Li, *et al.*, Unravelling the mechanism of ionic fullerene passivation for efficient and stable methylammonium-free perovskite solar cells, *ACS Energy Lett.*, 2020, **5**(6), 2015–2022.
163 B. L. Watson, N. Rolston, K. A. Bush, T. Leijtens, M. D. McGehee and R. H. Dauskardt, Cross-linkable, solvent-resistant fullerene contacts for robust and efficient perovskite solar cells with increased J sc and V oc, *ACS Appl. Mater. Interfaces*, 2016, **8**(39), 25896–25904.
164 B. Li, *et al.*, Steering the electron transport properties of pyridine-functionalized fullerene derivatives in inverted perovskite solar cells: The nitrogen site matters, *J. Mater. Chem. A*, 2020, **8**(7), 3872–3881.
165 R. Lin, *et al.*, Monolithic all-perovskite tandem solar cells with 24.8% efficiency exploiting comproportionation to suppress Sn (ii) oxidation in precursor ink, *Nat. Energy*, 2019, **4**(10), 864–873.
166 K. Yan, *et al.*, A multifunctional and scalable fullerene electron transporting material for efficient inverted perovskite solar cells and modules, *Sci. China: Chem.*, 2023, **66**(6), 1795–1803.
167 S. V. Bhosale, M. Al Kobaisi, R. W. Jadhav, P. P. Morajkar, L. A. Jones and S. George, Naphthalene diimides: perspectives and promise, *Chem. Soc. Rev.*, 2021, **50**(17), 9845–9998.
168 Q. Chen, W. Wang, S. Xiao, Y.-B. Cheng, F. Huang and W. Xiang, Improved performance of planar perovskite solar cells using an amino-terminated multifunctional fullerene derivative as the passivation layer, *ACS Appl. Mater. Interfaces*, 2019, **11**(30), 27145–27152.
169 M. Zhang, *et al.*, Reconfiguration of interfacial energy band structure for high-performance inverted structure perovskite solar cells, *Nat. Commun.*, 2019, **10**(1), 4593.
170 L. Jia, B. Li, Y. Shang, M. Chen, G.-W. Wang and S. Yang, Double fullerene cathode buffer layers afford highly efficient and stable inverted planar perovskite solar cells, *Org. Electron.*, 2020, **82**, 105726.
171 Q. Chen, C. Wang, Y. Li and L. Chen, Interfacial dipole in organic and perovskite solar cells, *J. Am. Chem. Soc.*, 2020, **142**(43), 18281–18292.
172 E. Voroshazi, *et al.*, Novel bis-C_{60} derivative compared to other fullerene bis-adducts in high efficiency polymer photovoltaic cells, *J. Mater. Chem.*, 2011, **21**(43), 17345–17352.
173 Y. Xing, C. Sun, H.-L. Yip, G. C. Bazan, F. Huang and Y. Cao, New fullerene design enables efficient passivation of surface traps in high performance pin heterojunction perovskite solar cells, *Nano Energy*, 2016, **26**, 7–15.
174 Z. Zhu, C. C. Chueh, F. Lin and A. K. Y. Jen, Enhanced ambient stability of efficient perovskite solar cells by employing a modified fullerene cathode interlayer, *Adv. Sci.*, 2016, **3**(9), 1600027.
175 J. Xie, *et al.*, Improved performance and air stability of planar perovskite solar cells via interfacial engineering using a fullerene amine interlayer, *Nano Energy*, 2016, **28**, 330–337.
176 B. Li, *et al.*, Anchoring fullerene onto perovskite film via grafting pyridine toward enhanced electron transport in high-efficiency solar cells, *ACS Appl. Mater. Interfaces*, 2018, **10**(38), 32471–32482.
177 Z. Xing, *et al.*, Multifunctional molecular design of a new fulleropyrrolidine electron transport material family engenders high performance of perovskite solar cells, *Adv. Funct. Mater.*, 2021, **31**(51), 2107695.
178 N. Cates, *et al.*, Molecular packing and solar cell performance in blends of polymers with a bisadduct fullerene, *Nano Lett.*, 2012, **12**(3), 1566–1570.
179 M. Vasilopoulou, *et al.*, Molecular materials as interfacial layers and additives in perovskite solar cells, *Chem. Soc. Rev.*, 2020, **49**(13), 4496–4526.
180 Y. Wang, *et al.*, Pyridine–functionalized fullerene derivative as an independent electron transport layer enabling efficient and hysteresis–free regular perovskite solar cells, *Nano Sel.*, 2021, **2**(11), 2192–2200.
181 B. Li, *et al.*, Efficient and stable tin perovskite solar cells by pyridine–functionalized fullerene with reduced interfacial energy loss, *Adv. Funct. Mater.*, 2022, **32**(39), 2205870.
182 H. Cheng, X. Zang, S. Wang and B. Cai, Pyridine–Functionalized Organic Molecules in Perovskite Solar Cells: Toward Defects Passivation and Charge Transfer, *Sol. RRL*, 2025, **9**(2), 2400736.
183 Y. Sun, Y. Lai and Y. Yang, Progress of Hole–Transport Layers in Mixed Sn–Pb Perovskite Solar Cells, *Small*, 2024, **20**(49), 2406991.
184 J. Zhen, *et al.*, Pyridine-functionalized fullerene additive enabling coordination interactions with $CH_3NH_3PbI_3$ perovskite towards highly efficient bulk heterojunction solar cells, *J. Mater. Chem. A*, 2019, **7**(6), 2754–2763.
185 B. Roy, T. Dey, S. Bose, S. Mahato, N. C. Das and S. K. Ray, Superior Photoconversion Efficiency of Nanocrystal Sensitized Solar Cells Based on All-Inorganic $CsPbX_3$ (X= Br, I) Perovskites, *Nanoscale*, 2025, **17**, 10743–10751.
186 S. Wang, *et al.*, Targeted therapy for interfacial engineering toward stable and efficient perovskite solar cells, *Adv. Mater.*, 2019, **31**(41), 1903691.
187 L. L. Deng, S. Y. Xie and F. Gao, Fullerene–Based Materials for Photovoltaic Applications: Toward Efficient,

Hysteresis–Free, and Stable Perovskite Solar Cells, *Adv. Electron. Mater.*, 2018, **4**(10), 1700435.

188 J. Li, M. Chen, S. Zhou, H. Li and J. Hao, Self-assembly of fullerene C_{60}-based amphiphiles in solutions, *Chem. Soc. Rev.*, 2022, **51**(8), 3226–3242.

189 X. Tong, *et al.*, Synergistically manipulating the shape of alkyl-chain and asymmetric side groups of non-fullerene acceptors enables organic solar cells to reach 18.5% efficiency, *Giant*, 2024, **19**, 100294.

190 Y. C. Wang, *et al.*, Terpyridine-zinc(II) coordination nanosheets as modulators of perovskite crystallization to enhance solar cell efficiency, *J. Mater. Chem. A*, 2023, **11**(13), 7077–7084.

191 D. Yadav, *et al.*, Stimuli-responsive biomaterials for tissue engineering applications, *Curr. Pharm. Biotechnol.*, 2024, **25**(8), 981–999.

192 D. M. Guldi, G. A. Rahman, V. Sgobba and C. Ehli, Multifunctional molecular carbon materials—from fullerenes to carbon nanotubes, *Chem. Soc. Rev.*, 2006, **35**(5), 471–487.

193 H. Wang, *et al.*, Halogen-substituted fullerene derivatives for interface engineering of perovskite solar cells, *J. Mater. Chem. A*, 2018, **6**(43), 21368–21378.

194 S. Hu, J. Thiesbrummel, J. Pascual, M. Stolterfoht, A. Wakamiya and H. J. Snaith, Narrow Bandgap Metal Halide Perovskites for All-Perovskite Tandem Photovoltaics, *Chem. Rev.*, 2024, **124**(7), 4079–4123.

195 D. P. McMeekin, *et al.*, Crystallization Kinetics and Morphology Control of Formamidinium–Cesium Mixed-Cation Lead Mixed-Halide Perovskite via Tunability of the Colloidal Precursor Solution, *Adv. Mater.*, 2017, **29**, 1607039.

196 L. Hong, *et al.*, Simultaneous improvement of efficiency and stability of organic photovoltaic cells by using a cross–linkable fullerene derivative, *Small*, 2021, **17**(24), 2101133.

197 T. Kang, *et al.*, Interfacial engineering with cross-linkable fullerene derivatives for high-performance perovskite solar cells, *ACS Appl. Mater. Interfaces*, 2017, **9**(44), 38530–38536.

198 F. Giacalone and N. Martín, New concepts and applications in the macromolecular chemistry of fullerenes, *Adv. Mater.*, 2010, **22**(38), 4220–4248.

199 Y. Wang, X. Wang, Z. Ding, Y. Wang and W. Huang, Cross-linking strategies for efficient and highly stable perovskite solar cells, *J. Mater. Chem. C*, 2023, **12**, 351–387.

200 A. Cabrera-Espinoza, S. Collavini, J. G. Sánchez, I. Kosta, E. Palomares and J. L. Delgado, Photo-Cross-Linked Fullerene-Based Hole Transport Material for Moisture-Resistant Regular Fullerene Sandwich Perovskite Solar Cells, *ACS Appl. Mater. Interfaces*, 2024, **16**(16), 20852–20864.

201 A. Diacon, L. Derue, C. Lecourtier, O. Dautel, G. Wantz and P. Hudhomme, Cross-linkable azido C_{60}-fullerene derivatives for efficient thermal stabilization of polymer bulk-heterojunction solar cells, *J. Mater. Chem. C*, 2014, **2**(35), 7163–7167.

202 D. A. García-Hernández, R. Barzaga, A. Manchado and F. Cataldo, Fullerene-indene adducts (ICMA & ICBA) in an astrochemical perspective part 1: chemical thermodynamics, stability and electronic absorption spectroscopy, *Fullerenes, Nanotubes Carbon Nanostruct.*, 2023, **31**(9), 897–905.

203 R. M. Faisal, *Buckyball Derivatives as Acceptors in Organic Photovoltaics, A Review*, 2022, vol. 13, no. 1, pp. 119–149.

204 Y. Shi, Z. Zhu, D. Miao, Y. Ding and Q. Mi, Interfacial Dipoles Boost Open-Circuit Voltage of Tin Halide Perovskite Solar Cells, *ACS Energy Lett.*, 2024, **9**(4), 1895–1897.

205 T. Ji, *et al.*, Charge transporting materials for perovskite solar cells, *Rare Met.*, 2021, **40**(10), 2690–2711.

206 B. Ali, F. Almyahi and M. A. Mahdi, Effect of Poly (3-Hexylthiophene): Mixed Fullerene Indene-C_{60} Multi-Adducts Ratios on the Performance of Organic Solar Cells, *Iran. J. Mater. Sci. Eng.*, 2023, **20**(2), 1–14.

207 J. Marin-Beloqui, *et al.*, Insight into the origin of trapping in polymer/fullerene blends with a systematic alteration of the fullerene to higher adducts, *J. Phys. Chem. C*, 2022, **126**(5), 2708–2719.

208 J. Qiu and S. Yang, Material and Interface Engineering for High–Performance Perovskite Solar Cells: A Personal Journey and Perspective, *Chem. Rec.*, 2020, **20**(3), 209–229.

209 Y. Xie, H. Lu, J. Huang and H. Xie, Natural materials for sustainable organic solar cells: status and challenge, *Adv. Funct. Mater.*, 2023, **33**(15), 2213910.

210 Y. Li, S. Yang, S. Yan, X. Liu, G. Shi and T. He, Open–Circuit Voltage Loss Management for Efficient Inverted Wide–Bandgap Perovskite Photovoltaics, *Adv. Funct. Mater.*, 2025, **35**(7), 2415331.